LIQUEFACTION OF URANIUM TAILINGS

(AECB Project No. 5.130.1)

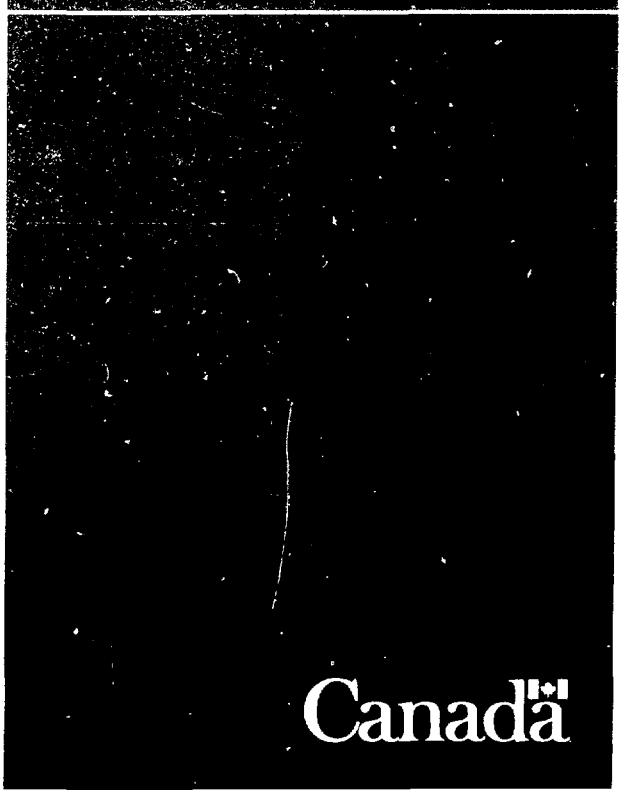

INFO-0409

Atomic Energy Control Board
P.O. Box 1046
Ottawa, Canada
K1P 5S9

Commission de contrôle de l'énergie atomique
C.P. 1046
Ottawa, Canada
K1P 5S9

LIQUEFACTION OF URANIUM TAILINGS

(AECB Project No. 5.130.1)

by

Acres International Ltd.

A research report prepared for the
Atomic Energy Control Board
Ottawa, Canada

Published February 1992

Canada

Research report

LIQUEFACTION OF URANIUM TAILINGS

A report prepared by Acres International Ltd., under contract to the Atomic Energy Control Board.

ABSTRACT

Numerical methods for assessing the liquefaction potential of soils are reviewed with a view to their application to uranium tailings. The methods can be divided into two categories: total stress analysis, where changes in pore pressure are not considered in the soil model, and effective stress analysis, where changes in pore pressure are included in the soil model. Effective stress analysis is more realistic, but few computer programs exist for such analysis in two or three dimensions. A simple linearized, two-dimensional, finite element effective stress analysis which incorporates volumetric compaction due to shear motion is described and implemented. The new program is applied to the assessment of liquefaction potential of tailings in the Quirke Mine tailings area near Elliot Lake, Ontario. The results are compared with those of a total stress analysis. Both analyses indicate liquefaction would occur if a magnitude 6.0 earthquake were to occur near the area. However, the extent of liquefaction predicted by the effective stress analysis is much less than that predicted by the total stress analysis. The results of both methods are sensitive to assumed material properties and to the method used to determine the cyclic shear strength of the tailings. Further analysis, incorporating more *in situ* and/or laboratory data, is recommended before conclusions can be made concerning the dynamic stability of these tailings.

RÉSUMÉ

Le présent rapport examine les méthodes numériques utilisées pour évaluer la liquéfaction potentielle des sols dans le but de déterminer si ces méthodes sont applicables aux résidus d'uranium. Ces méthodes se divisent en deux catégories : l'analyse en contraintes totales où le modèle de sol ne tient pas compte des changements de pression interstitielle et l'analyse en contraintes effectives où le modèle de sol en tient compte. L'analyse en contraintes effectives est plus conforme à la réalité, mais il y a peu de programmes informatiques qui peuvent accomplir une telle analyse en deux ou trois dimensions. Le rapport donne une description et un exemple d'une simple analyse bidimensionnelle linéaire par éléments finis en contraintes effectives, qui comprend la compaction volumétrique à cause du cisaillement, le tout réalisé dans le cadre de la présente étude. Le nouveau programme est utilisé afin d'évaluer la liquéfaction potentielle des résidus de l'aire de résidus de la mine Quirke, près d'Elliot Lake (Ontario). Les résultats ont été comparés avec ceux d'une analyse en contraintes totales. Les deux analyses indiquent que la liquéfaction aurait lieu si un tremblement de terre d'une magnitude de 6,0 survenait dans les environs. Or, la liquéfaction prévue par l'analyse en contraintes effectives est beaucoup moins étendue que dans le cas de l'analyse par contraintes totales. Les résultats de deux méthodes sont influencés par les caractéristiques attribuées aux sols et par la méthode utilisée pour déterminer la résistance au cisaillement cyclique des résidus. Le rapport recommande d'entreprendre des analyses supplémentaires, comprenant plus de données relevées sur les lieux ou en laboratoire, ou les deux, avant qu'on puisse arriver à des conclusions sur la stabilité dynamique des résidus en question.

ACKNOWLEDGEMENTS

The work reported herein could not have been accomplished without the help of two individuals. Particular acknowledgements go to Mr. Son Nguyen of the Atomic Energy Control Board in Ottawa who initiated the study, provided general advice and made many useful comments on the draft report. In addition to reviewing the draft report and providing technical guidance, Dr. Vinod Garga of the University of Ottawa helped to interpret the available *in situ* and laboratory tests so that a rational liquefaction analysis could proceed.

TABLE OF CONTENTS

LIST OF FIGURES

LIST OF TABLES

LIST OF SYMBOLS

Symbol	Definition
C_N	correction factor for measured blow count $N_1 = C_N N$
$\mathbf{c}$	element damping matrix
$\mathbf{C}$	global damping matrix
D_r	relative density
e	void ratio
$\mathbf{f}$	global force vector
g	acceleration due to gravity
G	shear modulus
G_0	shear modulus at small strain
k	permeability
K_0	coefficient of lateral earth pressure at rest
K_2	shear modulus coefficient at low strain
K_d	drained bulk modulus
$\mathbf{k}$	element stiffness matrix
$\mathbf{K}$	global stiffness matrix
M	fluid bulk modulus in saturated porous medium
$\mathbf{m}$	element mass matrix
$\mathbf{M}$	global mass matrix
n	porosity
N	measured blow count in standard penetration test
N_1	standardized blow count for standard penetration test
p	pore pressure
P_a	atmospheric pressure
u_i	ith component of displacement of solid skeleton
$\mathbf{u}$	nodal displacements
w_i	ith component of displacement of pore fluid with respect to solid skeketon
α	factor expressing compressibility of solid skeleton in saturated porous medium
ϵ	$= \epsilon_{ii}$
ϵ^p	inelastic volumetric strain
ϵ_{ij}	component of strain
γ	shear strain (sometimes unit weight)
λ	Lamé constant
ν	Poisson's ratio
ρ	density
σ_i or σ_{ij}	component of stress
σ'_i or σ'_{ij}	component of effective stress
τ	shear stress
θ	$= w_{k,k} = \partial w_k / \partial x_k$
ω_1	circular frequency of fundamental mode
ξ	damping ratio

1.0 INTRODUCTION

Uranium is mined and processed in Elliot Lake, Ontario. The tailings from these operations are pumped via pipeline to natural basins and retained by engineered earth dams at the mouths of these basins. Typically, tailings leave a pipe and are transported in a stream which eventually terminates in a tailings pond. Coarse particles are deposited near the source whereas finer particles are carried into the pond.

The stability of these tailings in the event of an earthquake is an important issue in planning the proper long-term management of the wastes generated by uranium mining. This report deals with the development and application of state of the art techniques for the analysis of the potential of the tailings to liquefy during an earthquake.

1.1 Liquefaction and Dynamic Analysis of Soils

Although the dynamic behavior of granular soils involves several complex processes, its essential physical aspects can be qualitatively described in terms of two processes: volumetric compaction and pore pressure changes. Dynamic shear stresses and strains caused by the earthquake ground motion cause slip at grain to grain contacts in the soil. In dry soils this inter-grain slip can lead to significant volumetric compaction and an increase in effective or inter-grain stress. In saturated soils the volumetric compaction is resisted by pore water since the water cannot drain away in time to accommodate the volume change. This resistance results in a transfer of effective stress to the pore water, resulting in an increase in pore pressure. In the extreme, the pore pressures may increase to equal the effective stresses. The result is liquefaction, a complete loss of shearing resistance in the soil.

An essential component of the liquefaction process is slip between soil particles resulting in volumetric compaction. It follows, therefore, that a soil whose grains have significant cohesion will exhibit a resistance to liquefaction. This is true of silts and clays which have a high degree of plasticity or ability to undergo permanent deformation without cracking or crumbling.

Ishihara *et al* (1980) proposed that the plasticity index of a fine-grained soil, a measure of its cohesiveness, be used as an indicator of its liquefiability. They applied this concept to the assessment of the liquefiability of mine tailings. It was found that tailings consisting of silt and clay size particles of quartz and feldspar minerals had a low plasticity index. This was attributed to the lack of cohesion between particles composed of these minerals. Laboratory testing of these tailings in fact showed that their resistance to cyclic shear was low.

Exceptions to the above particular cases exist and are common. However, reasons for these exceptions can be found. For example, Ishihara *et al* (1980) show that mine tailings containing significant amounts of fine-grained mica particles are more resistant to liquefaction. The reason is that mica has an inherent cohesiveness. Therefore, it is apparent that the qualitative assessment of liquefaction potential must be done on a case-by-case basis. Generalizations are possible, but whether they apply to a particular situation must be established by in-situ and/or laboratory tests.

The quantitative description of dynamic soil behavior is vastly more complicated since the processes of volumetric compaction and pore pressure changes described above are coupled and interdependent. This

means that the dynamic stress-strain behavior of the soil is nonlinear. Nevertheless, significant advances in the ability to quantitatively model soil dynamic behavior have been made in the last two decades.

Dynamic analysis of soils can be broadly divided into two categories: total stress and effective stress methods. In total stress methods the soils are modeled as equivalent one phase solids and changes in pore pressure are not considered. In effective stress analysis, changes in pore pressure are computed. There exist variations of total stress and effective stress methods, giving rise to several different sub-categories. Both types of analysis can incorporate nonlinear stress-strain behavior. The pore pressure generation model in effective stress analyses can be either coupled to the soil material model or uncoupled. Table 1.1 gives one classification scheme for the various soil dynamics analysis methods.

TABLE 1.1

CLASSIFICATION OF SOIL DYNAMICS ANALYSIS METHODS

Total Stress Analysis

- Equivalent linear soil model
- Nonlinear soil model

Effective Stress Analysis

- Uncoupled - pore pressures generated separately
  - linear soil model
  - nonlinear soil model
- Coupled - pore pressures generated simultaneously
  - linear soil model
  - nonlinear soil model

1.2 Plan and Scope of Report

The application of total stress and effective stress analysis techniques to the prediction of the liquefaction potential of uranium tailings in the event of an earthquake is the subject of this report. The first part of the report reviews the literature dealing with total stress and effective stress analysis. Basic analysis algorithms are presented and available computer programs are discussed. Improvements in the state of practice of both total stress and effective stress analysis are then described and implemented in two new computer programs. Both computer programs are then applied to the analysis of the tailings disposal area at the Quirke Mine near Elliot Lake, Ontario. Finally, some conclusions and recommendations are given.

1.3 Finite Element Analysis of Soil Dynamics Problems

Dynamic finite element analysis of a soil deposit or structure is based on the matrix differential equation

$$\mathbf{M}\ddot{\mathbf{u}} + \mathbf{C}\dot{\mathbf{u}} + \mathbf{K}\mathbf{u} = \mathbf{f}(t) \tag{1.1}$$

where **M**, **C** and **K** are, respectively, mass, damping and stiffness matrices of the finite element model and **u** is a vector of nodal displacements. The dots denote differentiation with respect to time. Each of these matrices is of size n, the number of degrees of freedom in the model. The vector $\mathbf{f}(t)$ is the dynamic forcing function. Expressions for the element matrices of four-noded isoparametric quadrilaterals are given in Appendix I.

In three dimensions, if it is assumed that the base of the finite element model is uniformly subjected to the acceleration time histories $a_x(t)$, $a_y(t)$ and $a_z(t)$, then the forcing function becomes

$$\mathbf{f}(t) = -\mathbf{M}\left\{ a_x(t)\begin{bmatrix}1\\0\\0\\\vdots\\1\\0\\0\end{bmatrix} + a_y(t)\begin{bmatrix}0\\1\\0\\\vdots\\0\\1\\0\end{bmatrix} + a_z(t)\begin{bmatrix}0\\0\\1\\\vdots\\0\\0\\1\end{bmatrix}\right\} \tag{1.2}$$

where each of the vectors shown is of length n. The displacement **u** is then the relative displacement of the nodes with respect to the base.

Given the material properties of each element in the model, the mass and stiffness matrices are computed using standard techniques described in Zienkiewicz (1977), Bathe (1982) or Hughes (1987). Numerically integrated isoparametric elements, containing a variable number of nodes, are often used although older computer programs employ simpler elements. A common approximate formulation of the mass matrix is a 'lumped' mass matrix where all the mass of an element is assigned to its nodes. The result is a diagonal mass matrix which has some computational and storage advantages. With the present easy availability of storage and fast processors, lumped mass formulations are not really necessary.

The damping matrix is often computed as a linear combination of the mass and stiffness matrices with the damping ratio, ξ, used as a scale factor. This is known as Rayleigh damping. Since the damping ratio could vary from element to element, the damping matrix is defined at the element level. The particular form most commonly assumed is

$$\mathbf{c} = \xi\left(\omega_1\mathbf{m} + \frac{\mathbf{k}}{\omega_1}\right) \tag{1.3}$$

where ω_1 is the fundamental (lowest) natural frequency of the finite element model given by the solution to the eigenvalue problem

$$\mathbf{K}\mathbf{q}_1 = \omega_1^2\mathbf{M}\mathbf{q}_1$$

where $\mathbf{q}_1$ is the eigenvector or mode shape of the fundamental mode.

Several time-stepping solution algorithms for Equation 1.1 are possible. Usually implicit algorithms are used, wherein a system of equations is solved at each time step to obtain nodal motions (see Bathe, 1982, pp. 500-515; Hughes, 1987, chap. 9). For nonlinear material models, Equation 1.1 is typically rewritten for an

increment of displacement Δu and some type of iterative method is employed at each time step to solve for increments of nodal motions (see Bathe, 1982, pp. 547-552).

1.4 Simplified Analysis of Liquefaction Potential

Any analysis of a soil deposit to determine its liquefaction potential requires that a measure of its resistance to cyclic shear stresses (its strength) be obtained. In addition, a measure of the induced shear stress due to ground motion caused by an assumed design earthquake is required. Comparison of the strength with the induced stress then yields an indication of the liquefaction potential of the soil.

1.4.1 Induced Shear Stress

Seed and Idriss (1971) developed a simplified method for computing the maximum shear stress within a soil deposit due to an earthquake. Assuming that the soil column above a soil element at a depth h behaves as a rigid body. The maximum shear stress on the soil element is then given by

$$\tau_{max} = \gamma h a_{max} \tag{1.4}$$

where γ is the unit weight of the soil and a_{max} is the peak ground acceleration at the surface measured in units of g, the acceleration due to gravity.

Since the soil column behaves as a deformable body, the shear stress at depth h will be less than that computed by Equation 1.4. Using ground response analysis of a number of different soil profiles, Seed and Idriss (1971) found that a reduction factor had to be applied to Equation 1.4 in order to obtain a more realistic measure of τ_{max}. Thus Equation 1.4 is rewritten as

$$\tau_{max} = \gamma h a_{max} r_d \tag{1.5}$$

The variation of this reduction factor with depth is shown in Figure 1.1. For depths greater than 40 ft. (12 m.) the range of possible values of r_d is large. However, an average curve may be assumed for depths less than 40 ft.

Generally, the shear stress time history at any point within a soil deposit will be highly irregular. For purposes of determining liquefaction potential, some measure of equivalent uniform average stress is necessary. Lee and Chan (1972) and Seed *et al* (1975) found that, to a reasonable degree of accuracy, the effect of a non-uniform shear stress time history on a soil sample is the same as that of a regular sinusoidal shear stress time history whose amplitude is 65% of the peak amplitude of the irregular time history. This amplitude is known as the average stress. Thus, the average stress generated within a soil deposit by an earthquake is given by

$$\tau_{av} = 0.65\tau_{max} = 0.65\gamma h a_{max} r_d \tag{1.6}$$

1.4.2 Cyclic Shear Strength

Tests to determine the resistance of soils to cyclic shear may be done either in the laboratory or in the field. Laboratory tests, such as the simple shear or triaxial tests, measure the amount of shear stress required to either induce large cyclic deformations or to cause the pore pressure to increase to equal the effective

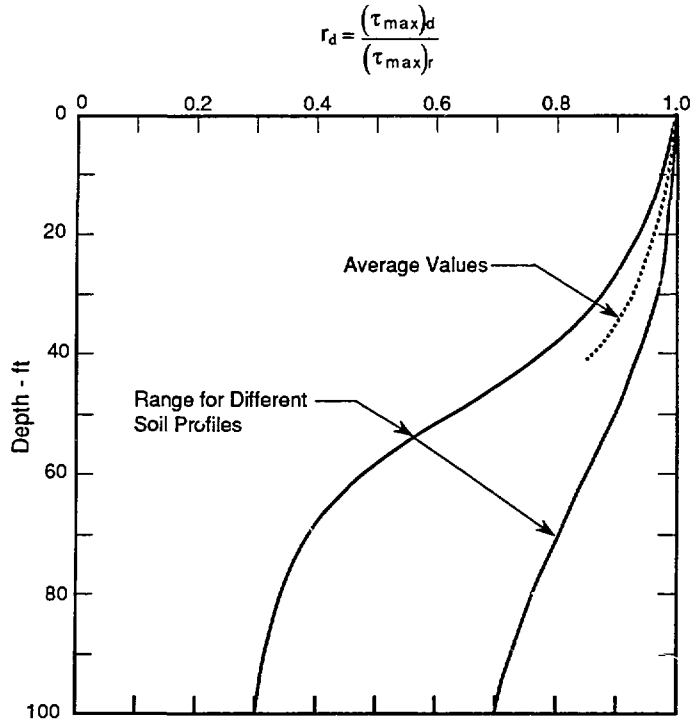

Source: Seed and Idriss, 1982

Fig. 1.1

Atomic Energy Control Board
Liquefaction of Uranium Tailings

Variation of Shear Stress Reduction Factor with Depth

P9296.00ES

confining pressure. Either of these occurrences denotes the onset of liquefaction. (Seed and Lee, 1966; Seed and Peacock, 1971)

Field determination of liquefaction resistance is based on empirical correlations between a soil characteristic measured in situ and observed performance. The most common field measurement is the standard penetration test (SPT) in which the measured soil characteristic is the number of blows of a 140 lb. hammer falling freely 30 in. required to drive a standard sampling tube (2 in. OD, 1.5 in. ID) 12 in. into the ground.

Following the 1964 Alaska and Niigata earthquakes, a number of investigators found correlations between the number of SPT blow counts at a particular depth, the presence or absence of liquefaction and

1) the effective vertical pressure at the depth,

2) the induced shear stress at the depth, and

3) the duration of significant shaking, and

4) the silt content of the soil

(see Kishida, 1966; Koizumi, 1966; Ohsaki, 1966; Seed and Peacock, 1971; Seed *et al*, 1983). For clean sands with little fines content, the first three of the above correlations have been subsumed into a set of curves known as SLAC (Seed Liquefaction Analysis Curves). These are shown in Figure 1.2.

The abscissa of the curves shown in Figure 1.2 is the standardized blow count, N_1 modified from the actual measured blow count N according to

$$N_1 = C_N N \tag{1.7}$$

where $C_N = (1/\sigma'_v)^{1/2}$ where σ'_v is measured in tons/ft^2 (Liao and Whitman, 1986). This standardization of the blow count eliminates the effect of confining pressure on the measured blow count. Field measurements of N are commonly performed using a standard equipment configuration described in Kovacs *et al* (1983) who estimated that 60% of the free-fall energy is transmitted to the drill rods of this configuration. Seed *et al* (1985) recommended adoption of this configuration as a standard. The resulting measured blow counts are therefore sometimes denoted N_{60} and the corrected blow counts are denoted $(N_1)_{60}$. In the following, it will be assumed that $N = N_{60}$ and $N_1 = (N_1)_{60}$.

The ordinate of the curves shown in Figure 1.2 is the lower bound of the cyclic shear resistance, $(\tau_{av}/\sigma'_v)_s$, required for no liquefaction at a particular value of N_1. The normalization by vertical effective stress eliminates the effect of confining pressure on the shear resistance. Finally, there is a different SLAC for different earthquake magnitudes because the duration of significant shaking increases with earthquake magnitude.

Given a design earthquake magnitude and an associated peak ground acceleration, the liquefaction potential at a particular depth in a soil deposit can be assessed by first determining the induced cyclic shear stress $(\tau_{av}/\sigma'_v)_e$ at the depth using Equation 1.6. The value of N_1 at the depth is then used to determine the shear resistance $(\tau_{av}/\sigma'_v)_s$. The factor of safety against liquefaction is then given by

$$FOS = \frac{(\tau_{av}/\sigma'_v)_s}{(\tau_{av}/\sigma'_v)_e} \tag{1.8}$$

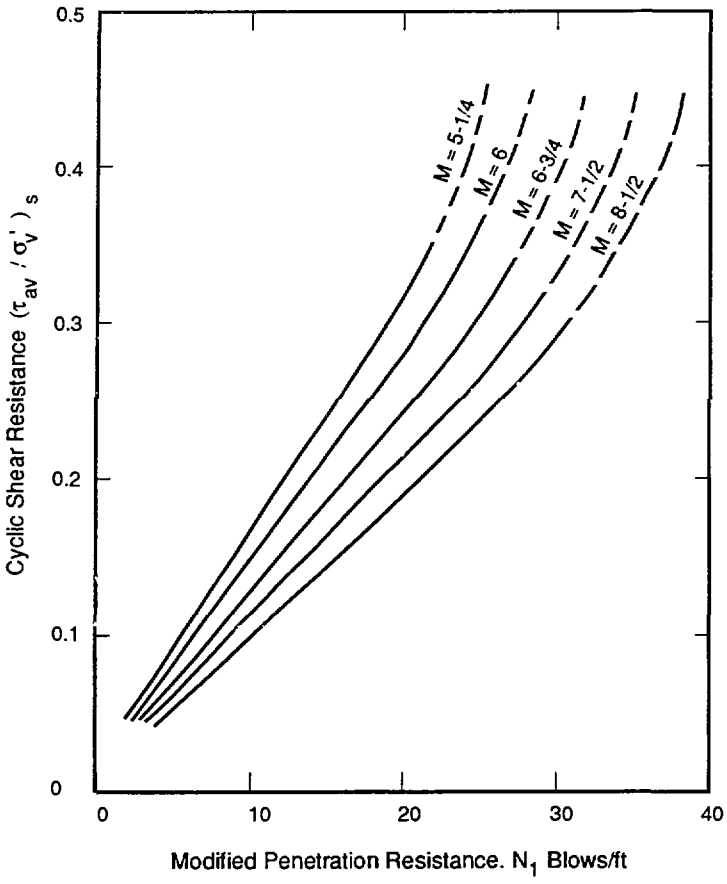

Source: Seed and Idriss, 1982

Fig. 1.2

Atomic Energy Control Board
Liquefaction of Uranium Tailings
Seed Liquefaction Analysis Curves

ACRES

P9296.00ES

This is the basis of a simplified method for evaluating liquefaction potential which employs only in-situ penetration tests and the simplified method for determining the induced shear stress described in Section 1.4.1. A more complete discussion of the method is given in Seed and Idriss (1982).

As mentionned previously, cyclic shear strength increases for soils with fine-grained particles exhibiting cohesion or plasticity. Since the SLAC are applicable to clean sands with little or no cohesion, the simplified method must be modified for application to cohesive soils with significant quantities of fines. Seed *et al* (1983) recommend incrementing values of N_1 by 7.5 to obtain an equivalent clean sand value. The SLAC could then be used to obtain the cyclic shear resistance. Zhou (1983) determined a similar value for the increment in N_1 based on the results of field studies in China. Tokimatsu and Yoshimi (1983) empirically the expression $0.1C + 4$ for the increment in N_1, where C is the content of fines in percent passing the #200 mesh (0.075 mm). It must be noted that these modifications only apply to natural deposits of silty soils; their application to a tailings deposit which does not exhibit cohesion or plasticity is questionable.

2.0 TOTAL STRESS ANALYSIS

2.1 Hyperbolic Stress-Strain Model

A fundamental component of several analysis methods currently in use is the hyperbolic stress-strain model of dynamic soil behavior. The basic concepts of this model are given below. Further details can be found in Kondner and Zelasko (1963), Duncan and Chang (1970), and Ishihara (1986).

The stress-strain relationship during the initial loading of a cyclic load sequence is given by

$$\tau = f(\gamma) \tag{2.1}$$

The curve f is called a skeleton or backbone curve and generally assumes a shape such as that shown in Figure 2.1. When the cyclic load reaches point A shown on Figure 2.1, a load reversal occurs along the lower (unloading) curve until the load reaches point B when another load reversal occurs along the upper (reloading) curve. The result is a hysteresis loop. The functional form of these hysteresis loops can be derived using the Masing rules (Pyke, 1979):

1) the slope of each load reversal curve (the shear modulus) assumes a value equal to the slope of the skeleton curve;

2) the shape of the unloading or reloading curves is the same as that of the initial loading curve, except that the scale is enlarged by a factor of two.

Given these rules, the load at each step is given by a shifted form of Equation 2.1

$$\frac{\tau \pm \tau_a}{2} = f\left(\frac{\gamma \pm \gamma_a}{2}\right) \tag{2.2}$$

where the plus sign applies to the reloading curve and the minus sign applies to the unloading curve.

If soil properties are assumed not to change during the progression of cyclic loading, then the stress-strain curve remains unchanged for constant amplitude unloading and reloading cycles. In such a case, the behavior of the soil can be characterized by a secant modulus, G, and a damping ratio, ξ

$$G = \frac{\tau_a}{\gamma_a} = \frac{f(\gamma_a)}{\gamma_a} \tag{2.3}$$

$$\xi = \frac{1}{4\pi}\frac{\Delta W}{W} \tag{2.4}$$

where ΔW is the damping energy, i.e., the unshaded area within the hysteresis loop shown in Figure 2.1, and W is the strain energy defined by

$$W = \frac{1}{2}\tau_a\gamma_a = \frac{1}{2}f(\gamma_a)\gamma_a \tag{2.5}$$

Since the hysteresis loop in Figure 2.1 is obtained by scaling the skeleton curve by two in both the γ and τ directions, the area ABA has the same shape as the area AOA. Hence the area ABA is four times the area of AOA. The unshaded area under the curve is therefore given by

$$\Delta W = 8\left[\int_0^{\gamma_a} f(\gamma)d\gamma - W\right] \tag{2.6}$$

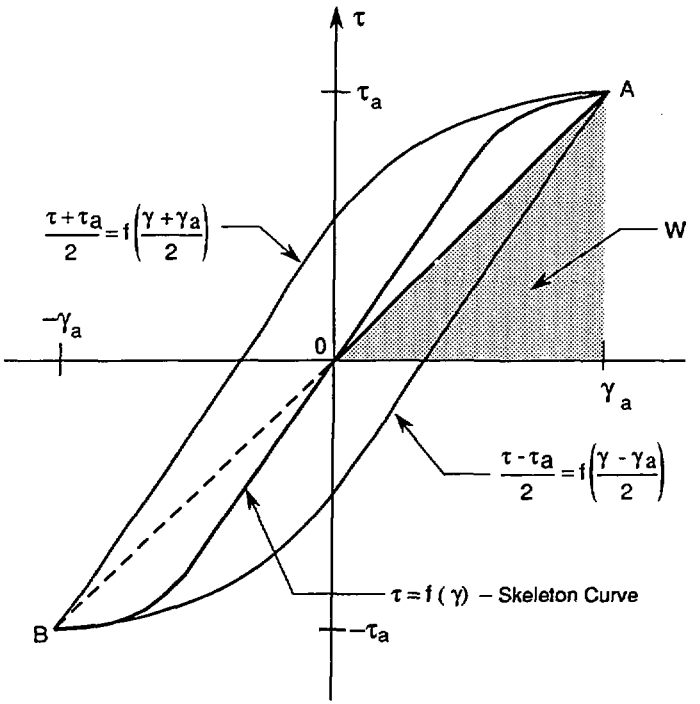

Fig. 2.1

Atomic Energy Control Board
Liquefaction of Uranium Tailings
Hyperbolic Stress - Strain Model

AGRES

P9296.00ES

Substitution of Equation 2.5 and 2.6 into Equation 2.4 gives

$$\xi = \frac{2}{\pi}\left[\frac{2\int_0^{\gamma_a} f(\gamma)d\gamma}{f(\gamma_a)\gamma_a} - 1\right] \tag{2.7}$$

Useful functional forms for G and ξ may be obtained using an equation for the hyperbolic skeleton curve suggested by Kondner and Zelasko (1963)

$$\tau = f(\gamma) = \frac{G_0\gamma}{1+\gamma/\gamma_r} \qquad \gamma > 0 \tag{2.8}$$

where G_0 is the initial shear modulus at $\gamma = 0$ and $\gamma_r = G_0\tau_f$ is the reference strain defined in terms of the shear strength, τ_f, of the soil. Using Equations 2.3 and 2.8, the secant modulus is given by

$$\frac{G}{G_0} = \frac{1}{1+\gamma_a/\gamma_r} \tag{2.9}$$

The ratio G/G_0 computed from Equation 2.9 is plotted versus γ_a/γ_r in Figure 2.2. Note that the modulus is reduced to half its initial value when the shear strain equals the reference strain.

An expression for the damping ratio can be derived by substituting Equation 2.8 into 2.7

$$\xi = \frac{4}{\pi}\left(1+\frac{1}{\gamma_a/\gamma_r}\right)\left[1 - \frac{1}{\gamma_a/\gamma_r}\ln\left(1+\frac{\gamma_a}{\gamma_r}\right)\right] - \frac{2}{\pi} \tag{2.10}$$

The variation of ξ with γ_a/γ_r is also shown in Figure 2.2. As γ_a/γ_r becomes large, ξ converges to $2/\pi$.

The above model and the underlying Masing rule assumptions describe the basic dynamic behavior of a soil. In reality, the behavior is more complex, particularly when different strain amplitudes occur during the loading, as in an earthquake. When the second of the Masing rules is applied in this case, the shear strength of the soil would be exceeded many times during an earthquake, a phenomenon which does not agree with observations. This problem has been discussed by Pyke (1979) and modifications to the theory, either in the form of additional Masing rules or completely different formulations, have been proposed (Pyke, 1979; Finn *et al*, 1977; Dikmen and Ghaboussi, 1984).

2.2 Equivalent Linear Elastic Algorithm

The non-linear effects which occur in soils during an earthquake can be approximated using a linear analysis, provided the stiffness and damping used in the analysis are compatible with the effective shear strain amplitudes. This approach was developed by Seed and Idriss (1969) and is called the equivalent linear method. In the following the basic algorithm and a pseudo code description is given.

The algorithm begins by estimating a shear modulus, G, and damping ratio, ξ, for each element of the model. The corresponding matrices $\mathbf{K}$ and $\mathbf{C}$ of Equation 1.1 are then computed and the equation is solved by a time-stepping algorithm. At each time step, the maximum shear strain in each element is computed. In two dimensions, this is given by

$$\gamma_m = [(\epsilon_{xx} - \epsilon_{yy})^2 + 4\epsilon_{xy}^2]^{1/2}.$$

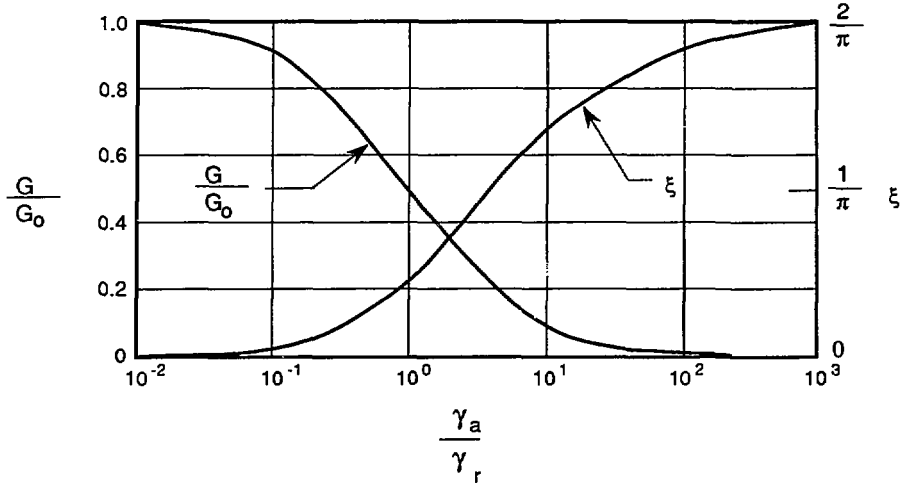

Fig. 2.2

Atomic Energy Control Board
Liquefaction of Uranium Tailings
Variation of Shear Modulus and Damping Ratio with Strain

ACRES

Pseudo-code for Equivalent Linear Algorithm

```
Set initial maximum shear strain γm in each element to zero.
Assign initial values of G and ξ to each element.
Compute matrix M of Equation 1.1.
For n = 1 to number of iterations
    Compute matrices C and K of Equation 1.1
    For i = 1 to number of time steps
        advance solution of Equation 1.1 by one time step
        For j = 1 to number of elements
            compute maximum shear strain γt
            if (γt > γmj) γmj = γt
        end j
    end i
    For j = 1 to number of elements
        compute G(γmj), ξ(γmj)
    end j
end n
```

The time history $\gamma_m(t)$ is monitored in each element to determine the peak value. The effective or average value of the maximum strain is given by

$$\gamma_{av} = 0.65 \max_t [\gamma_m(t)]$$

and this is used to compute new values of G and ξ for each element. The factor 0.65 is usually assumed based on the work of Seed *et al* (1975). The solution is then repeated with these new values. This process continues until the maximum percent change in shear modulus in each element is less than 10%, for example.

Curves relating G/G_0 and ξ to shear strain have been derived using experimental data from tests on sand and clay samples (Seed and Idriss, 1970; Seed *et al*, 1986). They are similar in shape to the curves given in Figure 2.2. For a logarithmic sequence of average shear strains, tabulated values of G/G_0 and ξ for sand and clay are given in Table 2.1. Given a value of γ_{av}, linear interpolation of G/G_0 or ξ versus $\log \gamma_{av}$ is commonly used to obtain values of G and ξ. The shear modulus at low strain, G_0, may be obtained from either geophysical methods in the field (Ballard and McLean, 1975) or by resonant column tests in the laboratory (Hardin and Drnevich, 1972).

In terms of the hyperbolic stress-strain model shown in Figure 2.1, the equivalent linear elastic model basically computes solutions to Equation 1.1 using different secant moduli and damping ratios compatible with the level of strain induced by the ground motion.

TABLE 2.1

STRAIN-COMPATIBLE SOIL PROPERTIES

		G/G_0		ξ	
γ_{av} (%)	$\log \gamma_{av}$	Sand	Clay	Sand	Clay
$\leq 10^{-4}$	-4.0	1.000	1.000	0.50	2.50
3.16×10^{-4}	-3.5	0.984	0.913	0.80	2.50
1.00×10^{-3}	-3.0	0.934	0.761	1.70	2.50
3.16×10^{-3}	-2.5	0.826	0.565	3.20	3.50
1.00×10^{-2}	-2.0	0.656	0.400	5.60	4.75
3.16×10^{-2}	-1.5	0.443	0.261	10.00	6.50
1.00×10^{-1}	-1.0	0.246	0.152	15.50	9.25
3.16×10^{-1}	-0.5	0.115	0.076	21.00	13.80
1.00	0.0	0.049	0.037	24.60	20.00
3.16	0.5	0.049	0.013	24.60	26.00
≥ 10.0	1.0	0.049	0.004	24.60	29.00

2.3 Available Computer Programs

The most widely used program for equivalent linear total stress analysis is SHAKE (Schnabel it et al , 1972). The program is one-dimensional and uses shear beam theory to compute transfer functions for each layer of a layered deposit. Complete time history analysis is performed using a given accelerogram. Soil moduli and damping ratios are modified according to the procedure described in Section 2.2.

For two-dimensional equivalent linear analysis the most popular program is QUAD-4 (Idriss it et al, 1973). QUAD-4 employs quadrilateral and triangular finite elements. A lumped mass formulation is used. The time integration scheme is one developed by Wilson and Clough (1962).

Two other finite element programs capable of equivalent linear analysis are LUSH (Lysmer *et al*, 1974) and FLUSH (Lysmer it et al, 1975). The key difference between these programs and QUAD-4 is the use of fast Fourier transforms to integrate the matrix differential equations, Equation 1.1. FLUSH is also capable of three-dimensional analysis and has an energy transmitting boundary which eliminates reflections from artificial boundaries of the finite element model. LUSH and FLUSH are often used for soil-structure interaction.

3.0 EFFECTIVE STRESS ANALYSIS

In effective stress analysis the changes in pore pressure which occur when a soil deposit is subjected to ground motion are taken into account. There is a variety of methods by which pore pressures can be modelled. The analysis may be coupled, i.e., treat the soil as a two-phase medium composed of a soil skeleton and pore water, or uncoupled where the response of the soil and pore water are treated separately. The assumed material model may be linear or non-linear, resulting in further variety.

The basic principles of existing effective stress analysis programs are described in the following sections.

3.1 Pore Pressure Generation Models

If a saturated soil is considered as a two-phase medium composed of a soil skeleton and pore water, two physical mechanisms are responsible for changes in pore pressure. One is the coupling between the soil skeleton and pore water which results in a transient pore pressure change. The other is the tendency for soils, particularly loose sands, to decrease in volume when subjected to shear strains. The volume decrease is resisted by the pore water resulting in an increase in pore pressure.

Soil is often represented as a series of solid particles with interconnecting saturated pores (see Figure 3.1). The particles are free to move in response to a dynamic load, but return to their original position at the end of the load time history. The water in the pores also responds to the load resulting in changes in pore pressure. Ground motion due to an earthquake is oscillatory in nature and consequently increases in pore pressure would tend to be cancelled by opposing decreases. This is depicted in Figure 3.1a. The result is that little or no net change in pore pressure at the end of the loading, i.e., residual pore pressures would be low and liquefaction would not be indicated.

Volumetric decrease is the principal mechanism of residual pore pressure generation in a saturated soil. This mechanism is illustrated in Figure 3.1b where the solid particles undergo permanent displacement in response to a dynamic load. The decrease in pore volume results in a net increase in pore pressure and possibly liquefaction. Effective stress analysis is concerned with modelling these volume changes by means of appropriate constitutive models.

Analysis of theoretical models and measurements on centrifuge models (Mansouri, 1980; Finn *et al*, 1984) confirm that the transient pore pressure changes in a soil due to coupling between the soil skeleton and pore water are much less significant than those due to volumetric changes.

The coupling between the soil skeleton and the pore water can be modelled by means of Biot's theory of the dynamic behavior of porous media (Biot, 1962). The pore pressure increases due to volumetric decrease can be modelled either by means of empirical relationships derived from laboratory data or by means of non-linear material models.

3.1.1 Coupled Soil-Water Model

Biot (1962) derived the following differential equations of motion for a coupled solid-fluid model:

$$\begin{aligned} \sigma_{ij,j} &= \rho \ddot{u}_i + \rho_f \ddot{w}_i \\ p_{,i} &= \rho_f \ddot{u}_i + \frac{1}{n}\rho_f \ddot{w}_i + \frac{1}{k}\dot{w}_i \end{aligned} \tag{3.1}$$

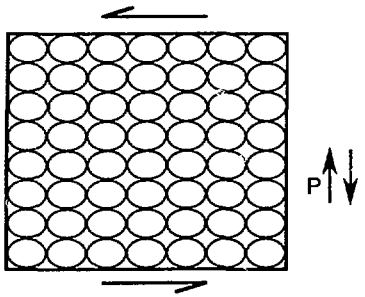

a. Wave Propagation

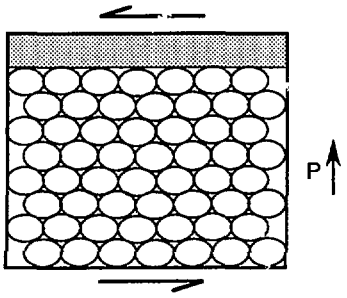

b. Densification

Fig. 3.1

Atomic Energy Control Board
Liquefaction of Uranium Tailings
Pore Pressure Generation Mechanisms

P9296.00ES

where u_i is a component of motion of the solid skeleton and w_i is a component of motion of the fluid with respect to the solid. The summation convention is assumed and the notation $f_{,i} = \partial f/\partial x_i$ where f is any variable. *The first equation is a statement of bulk equilibrium while the second is the generalized Darcy flow* law for a medium having a homogeneous isotropic permeability, k. The constitutive relationships for linear elastic media are

$$\sigma_{ij} = \lambda\epsilon\delta_{ij} + 2G\epsilon_{ij} + \alpha M(\alpha\epsilon + \theta)\delta_{ij} \tag{3.2a}$$

$$p = M(\alpha\epsilon + \theta) \tag{3.2b}$$

where $\epsilon = u_{k,k}$ and $\theta = w_{k,k}$. The Lamé constants λ and G are for drained conditions. The parameters M and α express the bulk fluid behavior and the compressibility of the solid skeleton respectively (see Appendix II). The above equations model wave propagation in the soil as well as the generation and dissipation of pore pressures due to Darcian flow through the soil. The equations do not model changes in pore pressure due to volumetric decrease. Therefore, although Equations 3.1 and 3.2 are a better representation of dynamic soil behavior, modifications must be made to the constitutive model to include the effects of volumetric decrease.

A finite element discretization of a porous saturated solid would have solid and fluid displacement degrees of freedom at each node. The system of matrix differential equations corresponding to Equation 3.1 has been derived by Ghaboussi and Wilson (1972). The result is as follows:

$$\begin{bmatrix} \mathbf{M}_s & \mathbf{M}_c \\ \mathbf{M}_c^t & \mathbf{M}_f \end{bmatrix} \begin{bmatrix} \ddot{\mathbf{u}} \\ \ddot{\mathbf{w}} \end{bmatrix} + \begin{bmatrix} \mathbf{C}_s & 0 \\ 0 & \mathbf{C}_f \end{bmatrix} \begin{bmatrix} \dot{\mathbf{u}} \\ \dot{\mathbf{w}} \end{bmatrix} + \begin{bmatrix} \mathbf{K}_s & \mathbf{K}_c \\ \mathbf{K}_c^t & \mathbf{K}_f \end{bmatrix} \begin{bmatrix} \mathbf{u} \\ \mathbf{w} \end{bmatrix} = \begin{bmatrix} \mathbf{f}(t) \\ 0 \end{bmatrix} \tag{3.3}$$

where $\mathbf{f}(t)$ is given by Equation 1.2 and the superscript t denotes the transpose. The subscripts s and f denote, respectively, quantities related to the solid and fluid. Equation 3.3 has a straightforward physical interpretation, there being a system of equations for motion of the solid and another for motion of the fluid. The matrices $\mathbf{M}_c$ and $\mathbf{K}_c$ express the coupling between the solid and fluid. Expressions for the element solid, fluid and coupling matrices are given in Appendix I.

The damping matrix, $\mathbf{C}_s$, represents the energy dissipated in the solid skeleton. Assuming Rayleigh damping, Ghaboussi and Wilson (1972) used the following linear combination of the mass and stiffness matrices of the solid skeleton for $\mathbf{C}_s$:

$$\mathbf{C}_s = \xi\omega_1(\mathbf{M}_s - n^2\mathbf{M}_f) + \frac{\xi}{\omega_1}(\mathbf{K}_s - \alpha^2\mathbf{K}_f) \tag{3.4}$$

where ξ is an assumed damping ratio and ω_1 is the fundamental frequency of the solid skeleton. The fundamental frequency is computed from the eigenvalue problem

$$(\mathbf{K}_s - \alpha^2\mathbf{K}_f)\mathbf{q}_1 = \omega_1^2(\mathbf{M}_s - n^2\mathbf{M}_f)\mathbf{q}_1. \tag{3.5}$$

3.1.2 Uncoupled Models

An uncoupled analysis treats the soil skeleton and pore fluid behavior separately. Generally, in these types of analyses, the shear stress history in the soil is computed by some type of total stress analysis The pore pressure increases due to volume decrease are incorporated by means of an empirical relationship while pore pressure changes due to Darcian flow are computed by a separate analysis, given the shear stress time history from the total stress analysis.

Two empirical models for pore pressure increase due to volume decrease are discussed below. Both are based on the assumption that earthquake loading is so rapid that undrained conditions prevail during the ground motion.

Seed *et al* (1976) and Martin and Seed (1979) developed an uncoupled analysis methodology based on observations of the rate of pore pressure increase in undrained cyclic loading tests. It was found that if the ratio p/σ_v' is plotted against the ratio N_e/N_l, where N_e is the number of cycles of stress applied and N_l is the number of cycles to initial liquefaction, the resulting curves fell into the narrow band shown in Figure 3.2. The method proceeds basically as follows: The shear stress time history provided by a ground response analysis is converted to N_e cycles of an equivalent uniform amplitude time history using a weighting scheme developed by Seed *et al* (1975). Alternatively, the design earthquake magnitude can be related to N_e (Seed *et al*, 1976). Knowing N_l from undrained cyclic loading tests on the soil and σ_v' for the depth in question, the pore pressure can be determined from curves such as that shown in Figure 3.2.

Pore pressures are evaluated by a separate analysis, given the shear stress time history. If desired, the resulting pore pressures can be used to adjust the material properties of the soil in the total stress analysis. This leads to an iterative process involving repeated total stress and pore pressure analyses until some convergence criterion is achieved. Usually only one iteration is done.

Although simple in principle, the disadvantage of the procedure described above is the large amount of bookkeeping and data transfer between programs required. The procedure has not been tried in a two-dimensional analysis.

Another empirical relationship between pore pressure increase and volume decrease is given in Martin *et al* (1975). The decrease in volume is caused by rearrangement of grains resulting in an increase in effective stress, i.e., an increase in pore pressure. It is shown in Appendix III that, under certain conditions, the increase in pore pressure, Δp is related to the volumetric strain of the soil skeleton, $\Delta\epsilon^p$, by the equation

$$\Delta p = K_d \Delta \epsilon^p \tag{3.6}$$

where $K_d = \lambda + \frac{2}{3}G$ is the bulk modulus of the drained soil (see Appendix II).

The volumetric strain can be computed by means of any constitutive theory. However, Martin *et al* (1975) found that the volumetric strain could be related to the current shear strain, γ, and the total accumulated volumetric strain, ϵ^p, as follows:

$$\Delta\epsilon^p = C_1(\gamma - C_2\epsilon^p) + \frac{C_3(\epsilon^p)^2}{\gamma + C_4\epsilon^p} \tag{3.7}$$

where the four constants C_1, C_2, C_3, and C_4 may be evaluated using data from constant strain amplitude cyclic tests. For a crystal silica sand sample, Martin *et al* (1975) found that

$$C_1 = 0.80 \quad C_2 = 0.79 \quad C_3 = 0.45 \quad C_4 = 0.73.$$

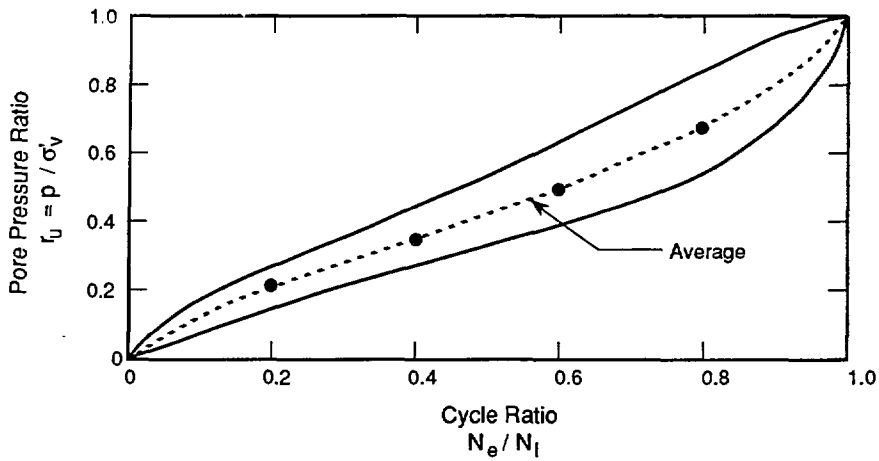

Source: De Alba et al, (1976)

Fig. 3.2

Atomic Energy Control Board
Liquefaction of Uranium Tailings
Pore Pressure Increase During Cyclic Simple Shear Tests

P9296.00ES

3.2 Non-Linear Effective Stress Models

Volumetric changes during cyclic loading can be accounted for by means of a non-linear material model derived by means of plasticity theory. Such models basically give rules for predicting the relationship between the shear stress τ and the effective stress σ' during cyclic loading (the effective stress path). The rules are essentially equations relating τ and σ' based on the observed laboratory behavior of soils subjected to cyclic shear stress under undrained conditions. This type of model was originally developed by Ishihara *et al* (1975) and subsequently refined (Ishihara and Towhata, 1980). Applications of these models in a coupled analysis are given in Ghaboussi and Dikmen (1978, 1984) and Prevost (1978, 1982).

Depending on the particular formulation, effective stress path models can be difficult to apply since they may require parameters which are not measured in general practice. Also, there is little verification of computer programs which incorporate these models.

An alternative is an uncoupled non-linear analysis which uses the hyperbolic stress-strain relationship described in Section 2.1 to model the loading and unloading behavior in the absence of pore pressure effects. Pore pressure effects are modelled using Equations 3.6 and 3.7. The connection between the pore pressure and shear modulus is provided by a hardening rule which relates shear stress to shear strain and effective stress. Applications of this model are described by Martin *et al* (1975), Lee and Finn (1975, 1978), Finn *et al* (1977) and Finn *et al* (1986).

3.3 Available Computer Programs

There are several one-dimensional effective stress computer programs available. Martin and Seed (1979) describe uncoupled analyses done using MASH (Martin, 1978) for non-linear total stress analysis and APOLLO (Martin and Seed, 1978) for computation of the pore pressures. A combination of SHAKE (Schnabel *et al*, 1972) and APOLLO has also been used for uncoupled analyses (Seed *et al*, 1976). Chugh and Von Thun (1985) used SHAKE with modified versions of APOLLO and GADFLEA (Booker *et al*, 1976) in a similar fashion. (Although GADFLEA is a two-dimensional program, it was used to compute pore pressures in column models.) The modifications to APOLLO and GADFLEA were made to prevent transmission of shear waves through a liquefied layer of soil.

Uncoupled non-linear one-dimensional models, which use Equations 3.6 and 3.7 to describe increases in pore pressure are DESRA-1 (Lee and Finn, 1975) and DESRA-2 (Lee and Finn, 1978). Coupled non-linear one-dimensional models have been implemented in CHARSOIL (Liou *et al*, 1977) and in LASS-IV (Dikmen and Ghaboussi, 1984).

Very few two and three-dimensional effective stress programs are available. DYNAFLOW (Prevost, 1983) is a large program capable of non-linear static and dynamic analysis of two and three-dimensional problems. Fully coupled effective stress analyses are possible with this program and a large family of plastic effective stress path models is available. Ferrito and Nakamoto (1984) have verified DYNAFLOW using laboratory test data. Some verification has been done using recorded motions on the Long Valley dam in California (Griffiths and Prevost, 1988). Although a good user's manual is provided, DYNAFLOW is a difficult program to use and the material models require several parameters which are not usually measured.

TARA-3 (Finn *et al*, 1986) is an uncoupled non-linear effective stress program which uses a material model similar to that of the DESRA programs mentionned above. TARA-3 requires few parameters, most of which are easily measured by laboratory or field tests. The code has been extensively verified (Finn *et al*, 1984; Finn, 1985, 1987). TARA-3 is not readily available and a user's manual for the program has not been written.

A linear coupled analysis, which includes the effects of pore pressure increase due to volume decrease, is decribed by Mansouri (1980) and Mansouri *et al* (1983). The analysis essentially combines Equations 3.3, 3.6 and 3.7. Although a code is not available, the method is well described in the references and can be implemented with relative ease.

4.0 THE STATE OF PRACTICE AND IMPROVEMENTS

4.1 Computer Program Development

Given the unavailability of a two or three-dimensional effective stress analysis program, it was originally decided to use suitably modified versions of QUAD-4 and GADFLEA to effect a two-dimensional uncoupled effective stress analysis similar to that described by Seed *et al* (1976) or Chugh and Von Thun (1985). Source codes of both these programs were therefore obtained.

It quickly became apparent that obtaining shear stress time histories in each element from QUAD-4 and then converting them to equivalent uniform amplitude shear stress time histories for use in GADFLEA would become a very complicated exercise. For example, GADFLEA requires shear stress amplitudes at nodes, whereas QUAD-4 computes shear stresses at the centroids of elements. The algorithm for transferring element stresses to nodal stresses is essentially one of bookkeeping. However, neither of these programs is well written and the required modifications would have been difficult to make and would likely have involved rewriting significant portions of both programs.

An alternative was to use a linear coupled analysis such as that described in Ghaboussi and Wilson (1973), Mansouri (1980) or Mansouri *et al* (1983). After consultation with AECB, it was decided to proceed with the implementation of a variant of the linear coupled effective stress analysis. The two main advantages of this approach are that the model is a more realistic representation of dynamic soil behavior and, once implemented, the resulting program could be modified to include nonlinear behavior.

The methodology is well described in the references. Expressions for the associated element mass, damping and stiffness matrices are given in both Ghaboussi and Wilson (1973) and Mansouri (1980). Based on these expressions, subroutines which computed these matrices in two dimensions were written. Existing time-stepping solution programs at Acres were combined with these subroutines to produce a working coupled linear effective stress program. The program, called NESAP (New Effective Stress Analysis Program) models the pore pressure increase due to volume decrease described by Equations 3.6 and 3.7. The details of the algorithm are provided in the next section.

Given NESAP, it was a simple matter to produce a total stress code, mainly by deleting subroutine calls and adding an iterative procedure as described in Section 2.2. This resulted in a program called NTSAP (New Total Stress Analysis Program), a more efficient and better written program than QUAD-4.

Both of these new programs are written in standard FORTRAN-77 and have been implemented in the DOS operating system on a microcomputer with a 80386 chip and a 80387 math coprocessor. NESAP requires more memory than NTSAP and, for some problems, a compiler capable of accessing more memory than the DOS 640 kilobyte limit may have to be used. The transfer of either of these programs to a VAX machine only requires changes to some file open statements.

4.2 Coupled Effective Stress Analysis Algorithm

Setting up the matrix differential equation of Equation 3.3 is relatively straightforward if uniform material properties are assumed in each element. The matrices $\mathbf{M}_c$, $\mathbf{M}_f$ and $\mathbf{C}_f$ are scalar multiples of the solid mass matrix, $\mathbf{M}_s$. Once the fluid stiffness matrix, $\mathbf{K}_f$, is computed, a multiple of the matrix is added to the

Pseudo-code for Linear Coupled Effective Stress Algorithm

Compute mass and stiffness matrices for solid skeleton.
Solve eigenvalue problem, Equation 3.5, for ω_1.
Compute matrices for Equation 3.3.
Specify elements where pore pressures are to be computed (n_p elements).
Set maximum shear strain γ_m in n_p elements to zero.
Set pore pressures p in n_p elements to zero.
For $i = 1$ to number of time steps
    advance solution of Equation 3.3 by one time step
    For $j = 1$ to n_p
        compute strains ϵ_{ij}, ϵ and θ
        compute $\Delta p = M(\alpha\epsilon + \theta)$
        $\gamma_{mj} = \max(|2\epsilon_{xy}|, \gamma_{mj})$
        $p_j = p_j + \Delta p$
    end j
end i
Set ϵ^p in n_p elements to zero.
For $i = 1$ to number of cycles
    For $j = 1$ to n_p
        compute $\Delta\epsilon^p$ by Equation 3.7
        $\epsilon^p_j = \epsilon^p_j + \Delta\epsilon^p$
        compute Δp by Equation 3.6
        $p_j = p_j + \Delta p$
    end j
end i

stiffness matrix of the solid skeleton. Another multiple of $\mathbf{K}_f$ forms the coupling matrix, $\mathbf{K}_c$. The damping matrix $\mathbf{C}_s$ is computed according to Equations 3.4 and 3.5.

Four degrees of freedom are possible at each node. At impermeable boundaries, the flow of water relative to the solid is set to zero. In the case of earthquake ground motion, the displacements at the base of the model are fixed and motions of the solid skeleton are relative to the base. A Newmark time integration scheme (Hughes, 1987, chap. 9) is used to solve the system of differential equations.

A list of elements in which pore pressures are to be computed is specified. During the time integration, pore pressures due to wave propagation in these elements are computed by means of Equation 3.2b. These pore pressures are accumulated to give a component of the residual pore pressure at the end of the ground motion.

Computation of the pore pressure increase due to volume decrease is complicated by the fact that Equation

3.7 applies to a complete cycle of shear strain with amplitude γ. To use the equation, it is necessary to convert the shear strain time history in an element to an equivalent, in terms of its effect on the soil, uniform amplitude time history. Seed *et al* (1976) provide a means for performing this. Examination of the effects of a number of earthquakes suggests that an equivalent uniform amplitude shear strain time history would have an amplitude of 65% of the maximum strain developed and a number of cycles which increases with earthquake magnitude. For example, the equivalent shear strain time history due to a M6.0 earthquake would have 5 cycles.

During the time integration, the shear strain time history $\gamma(t)$ is monitored to find its maximum. Given this, and the number of cycles, a simple post-processing routine can be used to compute the increase in pore pressure according to Equation 3.7.

A pseudo-code description of the linear coupled effective stress algorithm is given in the box above. As shown, the algorithm computes pore pressure time histories in specified elements. Liquefaction is assumed to occur when the induced pore pressure equals the effective stress in the element. Material properties of liquefied elements are not changed during the time integration.

4.3 Test of NESAP

Simon *et al* (1984) derived an analytical solution for one-dimensional wave propagation in a saturated porous medium. The solution was derived for the following boundary conditions:

$$\sigma_{xx}(0,t) = f(t)$$
$$p(0,t) = 0$$

Graphs of the solutions for the displacements $u_x(0,t)$ and and $w_x(0,t)$ and pressures $p(x,t)$ were obtained for the case where $f(t)$ is a unit step function. These were used to test NESAP.

A one-dimensional finite element model was constructed along the x axis using two-dimensional elements with fixed displacements in the y direction, i.e., only displacements of the solid and fluid in the x direction were allowed. The model was 50 units long. Displacements in both directions were fixed at $x = 50$. The model was long enough to avoid disturbance from reflections at $x = 50$ during the time interval of interest.

Two sets of material properties were used, one to test the solid and fluid displacement calculations, the other to test the fluid pressure calculations. These material properties are given in Table 4.1.

Graphs of solid and fluid displacements at $x = 0$ versus time were copied from Simon *et al* (1984). Using the first set of parameters in Table 4.1, NESAP was run and the displacements at $x = 0$ were recorded. The comparison between the computed solution and the analytical solution is shown in Figure 4.1a. The agreement between the two solutions is reasonable, the maximum relative error being 6%. The error decreased as more elements were used in the model.

The fluid pressure calculation was tested using the second set of parameters. A graph of fluid pressure versus x for $t = 0.075$ units were copied from Simon *et al* (1984). NESAP was run and the pressures at the centroid of each element were computed. The comparison between the computed solution and the analytical solution is shown in Figure 4.1b. Again the agreement is reasonable and improved as the number of elements in the model increased.

TABLE 4.1

NESAP TEST - MATERIAL PROPERTIES

(arbitrary units)

$\lambda = 833.3 \quad G = 1250.0 \quad \rho = 0.3060 \quad \rho_f = 0.2977 \quad n = 0.333 \quad k = 4.883 \times 10^{-3}$

Material 1: $\alpha = 1.0 \quad M = 1.201 \times 10^5$
used to test displacement calculation

Material 2: $\alpha = 0.667 \quad M = 1.385 \times 10^4$
used to test fluid pressure calculation

Velocity of compressional waves in porous medium

$$V_c = \sqrt{\frac{\lambda + 2G + \alpha^2 M}{\rho}}$$

4.4 Test of NTSAP

The manual supplied with the QUAD-4 computer program (Idriss *et al*, 1973) contains one example with numerical output. The example is a 100 ft. column of sand discretized into 20 elements (42 nodes), each 5 ft. in height. Vertical displacements are fixed at all nodes. The column is subjected to the horizontal Taft Lincoln tunnel accelerogram scaled to a peak acceleration of 0.15g.

Given the initial moduli assigned to each element, three iterations were required to reduce the maximum percent change in modulus to less than 10%. The profile of maximum shear stress in each element after the third iteration is shown in Figure 4.2.

The same problem was solved using NTSAP. Three iterations were also required to reduce the maximum percent change in modulus to less than 10%. The profile of maximum shear stress in each element is compared with that computed by QUAD-4 in Figure 4.2. The results are similar, but exhibit some differences at the top and bottom of the column.

There are at least three reasons for the observed differences:

1) The element used in NTSAP is a four node isoparametric quadrilateral (Bathe, 1982). The quadrilateral element used in QUAD-4 is made up of four triangular elements.

2) QUAD-4 uses lumped mass matrices while NTSAP uses consistent mass matrices.

3) The time-stepping solution algorithm used in NTSAP is a Newmark algorithm (Hughes, 1987, chap. 9) while that used in QUAD-4 is one developed by Wilson and Clough (1962).

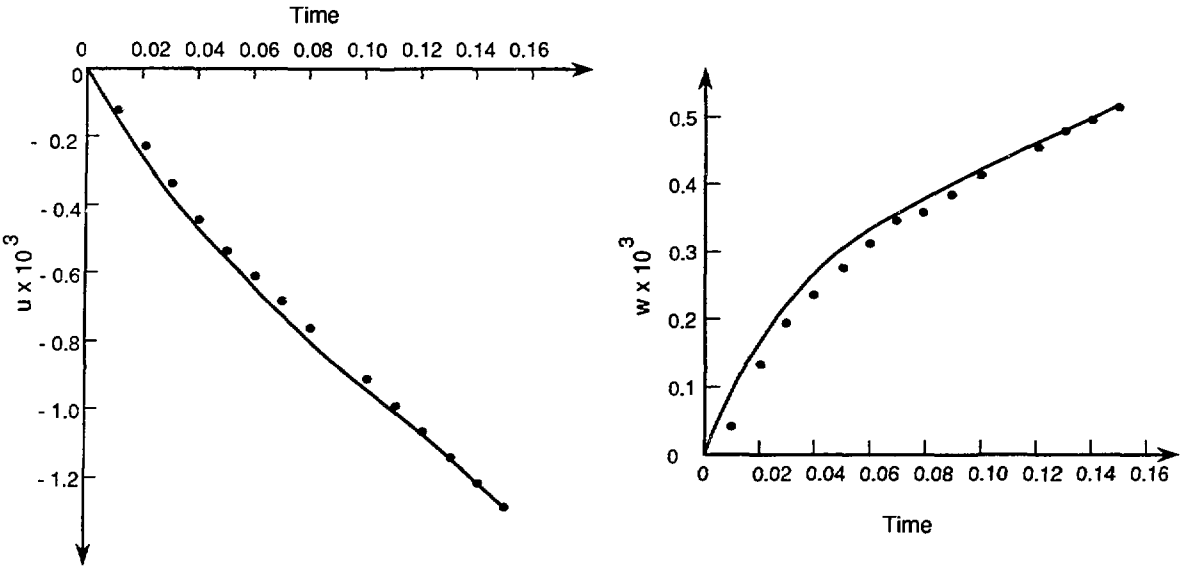

(a) Displacement Calculation (Arbitrary Units)

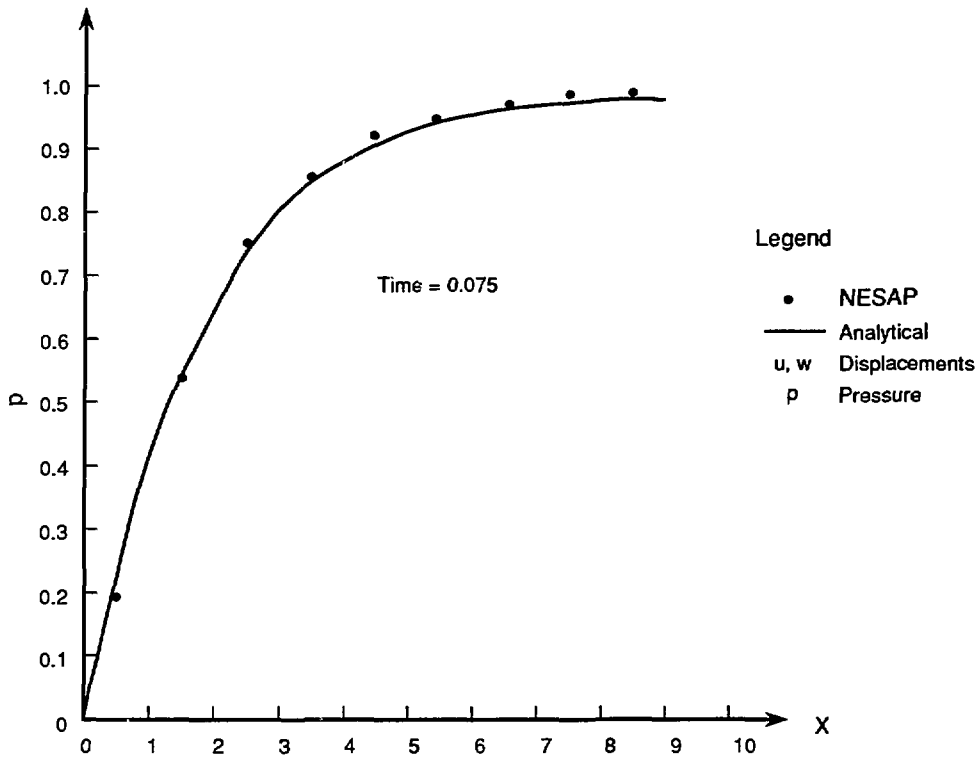

(b) Pressure Calculation (Arbitrary Units)

Fig. 4.1

Atomic Energy Control Board
Liquefaction of Uranium Tailings
Test of NESAP - Results

ACRES

P9296.00ES

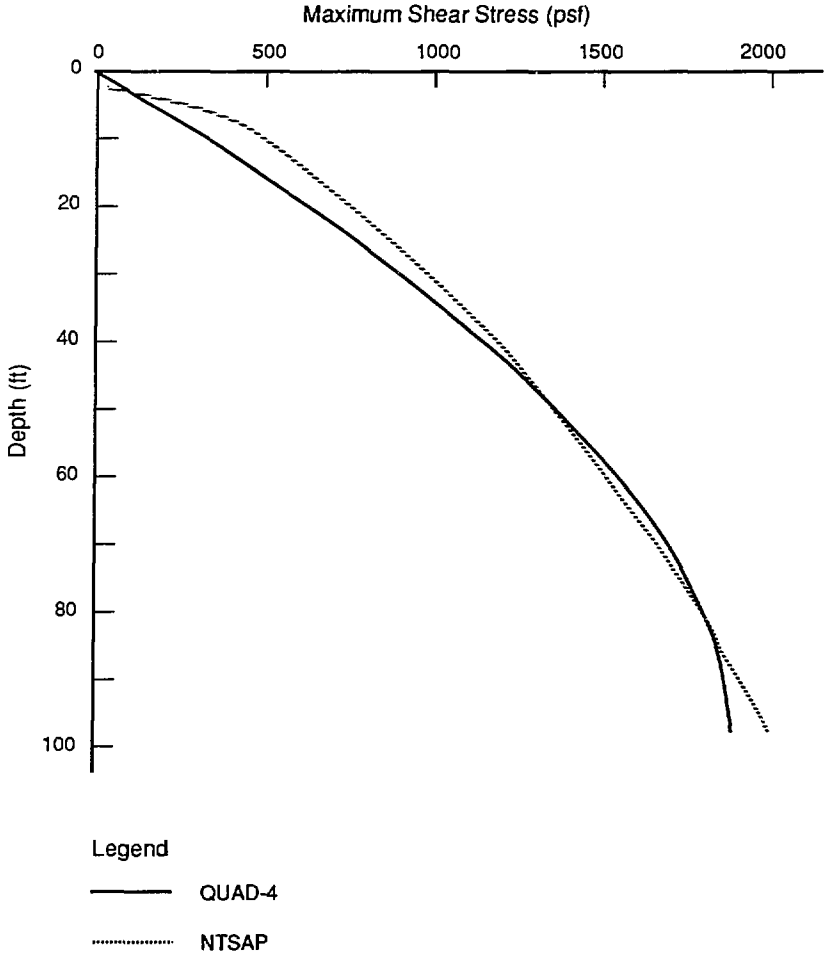

Fig. 4.2

Atomic Energy Control Board
Liquefaction of Uranium Tailings
Test of NTSAP - Results

P9296.00Es

Of these, the first two are probably the most significant. Despite the different element formulations, the computed resonant frequencies of the column at each iteration are similar, as shown below:

	ω_1 (rad/sec)	
Iteration	NTSAP	QUAD-4
1	9.763	9.758
2	9.719	9.501
3	9.689	9.426

It is not possible to determine which of the two programs is a 'better' representation of soil behavior. Given the comparison shown in Figure 4.2, both programs give results that are sufficiently similar for engineering purposes.

5.0 APPLICATION TO QUIRKE MINE TAILINGS DISPOSAL AREA

This chapter presents the results of the application of both total stress and effective stress analyses to the tailings disposal area at the Quirke Uranium Mine near Elliot Lake, Ontario. The computer procedures discussed in the previous chapter will be used.

5.1 Description of Quirke Mine Tailings Area

The Quirke Mine tailings disposal area is composed of several disposal ponds which occupy the old Manfred Lake valley. The tailings are produced during the milling process. Several dams and containment structures serve to contain tailings within the valley. The Main Dams shown in Figure 5.1 are two of such structures.

The geology underlying the Main Dams basically consists of about 25 m. of coarse-grained alluvium overlying bedrock. The alluvium is composed of glacio-fluvial materials ranging from sand to boulder sizes. The bedrock is mainly fluvially derived conglomerates. A thin layer of basal glacial till may overlie the bedrock.

Uranium production at the Quirke Mine, owned by Rio Algom Ltd., began in 1956 and stopped in 1961. The old Main Dam shown on Figure 5.1 was constructed from waste rock during this period. No production occurred during most of the 1960's. The mine was reactivated in August 1969. Approximately 20 million tonnes of tailings was produced during the period August 1969 to January 1979. Further expansion of the tailings area is necessary to accommodate the 29 million tonnes of tailings expected to be produced between 1979 and 1991. Geotechnical studies for this expansion have been undertaken by Golder Associates (1990).

Decommissioning of the tailings area may require the maintenance of an elevated water table within the tailings to minimize acid generation. To accommodate this, a new Main Dam was constructed to an elevation of 395 m. (1295 ft.). This dam is a zoned embankment dam comprised of a thick glacial till core and granular upstream and downstream shells with 2H:1V slopes. The final elevation of the tailings will be 393 m. (1290 ft.). The purpose of the analyses described in the next sections is to determine the liquefaction susceptibility of the tailings behind the new dam.

5.2 Assumed Accelerogram

The dynamic load used in both types of analysis is given by the north-south component of the St. André du Lac, Quebec accelerogram recorded during the November 25, 1988, M6.0 Saguenay earthquake. The peak ground acceleration of this accelerogram is 0.15g and it was recorded on rock at a distance of approximately 64 km from the epicenter of the earthquake.

The original accelerogram is a rather high frequency time history sampled at a time step of 0.005 sec. It is strongly suspected that there exists much high frequency noise (> 25 Hz) in this accelerogram. A crude filtering scheme was applied by resampling the original time history at a time step of 0.02 sec. The resulting accelerogram is shown in Figure 5.2.

In the report by Golder Associates (1990), it was assumed that the design earthquake was a M6.5 event located approximately 230 km from the site in the Western Quebec seismic zone. The corresponding peak acceleration was given as 0.065g. The duration of significant shaking was assumed to be less than 20

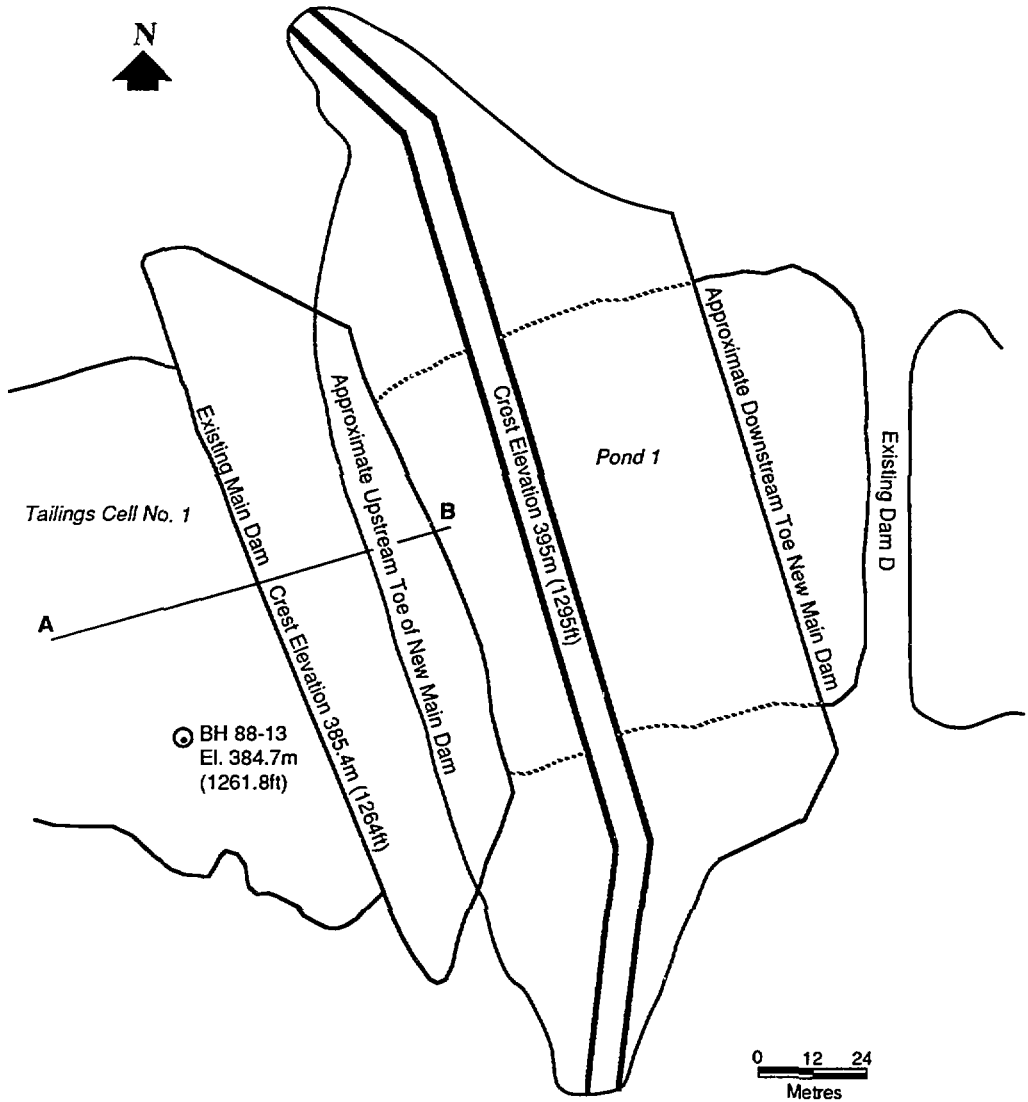

Source: Golder Associates (1990)

Fig. 5.1

Atomic Energy Control Board
Liquefaction of Uranium Tailings

Quirke Mine Tailings Disposal Area - Plan View of Main Dams

P9296.00Es

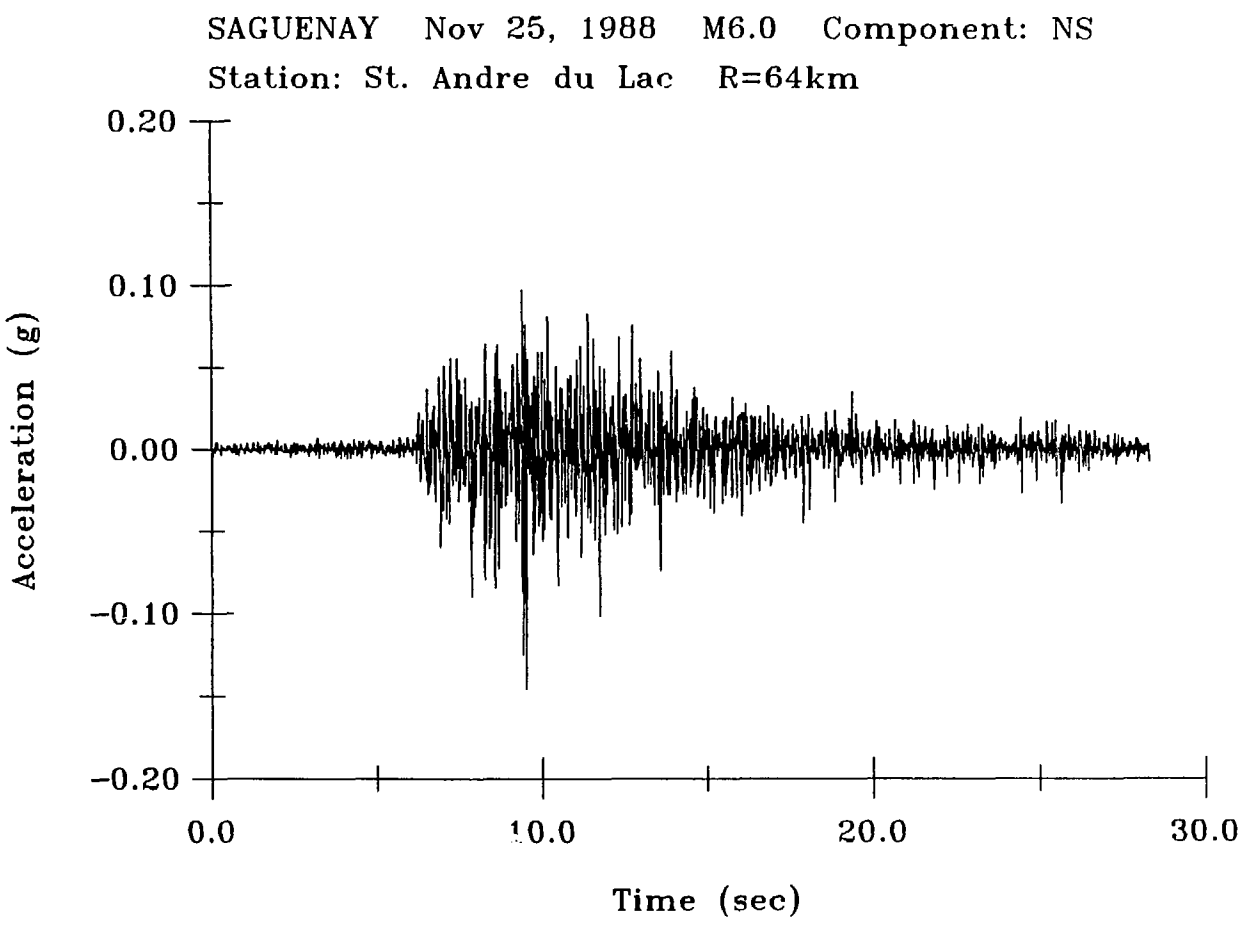

Fig. 5.2

Atomic Energy Control Board
Liquefaction of Uranium Tailings
Assumed Accelerogram

ACRES

seconds and the frequency content was assumed to range between 1 and 4 Hz. Except for its duration, the accelerogram shown in Figure 5.2 is not consistent with these design parameters.

The main reason for assuming the ground motion shown in Figure 5.2 is that the region surrounding the Quirke Lake mine lies in the same seismic zone as the region where the Saguenay earthquake occurred. However, as a result of the Saguenay earthquake, the seismic zonation of eastern Quebec is being reconsidered. No conclusions are available at present, but it is likely that the maximum magnitude for the region surrounding Quirke Lake will be less than M6.0. If so, the resulting ground motion would be of shorter duration than that shown in Figure 5.2. The amplitude would depend on the assumed location.

5.3 Total Stress Analysis

As described in Section 1.3, the determination of liquefaction susceptibility using a total stress procedure basically compares the shear stress ratio $(\tau_{av}/\sigma'_v)_s$ required to cause liquefaction (the 'strength') with an induced shear stress ratio $(\tau_{av}/\sigma'_v)_e$ caused by an assumed earthquake (the 'applied stress'). The factor of safety against liquefaction is then given by

$$FOS = \frac{(\tau_{av}/\sigma'_v)_s}{(\tau_{av}/\sigma'_v)_e}$$

The quantity $(\tau_{av}/\sigma'_v)_s$ can be obtained from cyclic shear or triaxial tests performed in the laboratory. It can also be obtained from Seed Liquefaction Analysis Curves shown in Figure 1.2. Both laboratory and field tests have been done on the tailings. However, as will be discussed below, only the field tests are useful.

The quantity $(\tau_{av}/\sigma'_v)_e$ may be computed using either Equation 1.6 or may be obtained from a total stress finite element analysis. Generally, where possible, it is best to compare two different approaches and this will be done.

5.3.1 Laboratory and Field Data

Cyclic triaxial tests of tailings samples taken from the Elliot Lake area were performed by Dr. Silver of the University of Illinois. The results of these tests are described in Silver (1980). These tests could have been used to determine cyclic stress ratios required to cause liquefaction. Unfortunately, the samples failed under their own weight and could not be directly inserted in a triaxial test chamber. All samples were therefore vacuum drained and remolded to obtain testable specimens. The results of the tests appear to reflect this sample preparation in that, for example, the measured strengths were found to be quite high considering the high water content and low density of the samples (Silver, 1980, p. 44). It was therefore concluded that the results of these tests are not useful.

Some standard penetration tests were performed in the tailings area and are likely more representative. The most representative profile of the final tailings pond is that of borehole BH 88-13 drilled during the 1988 investigation program (Golder Associates, 1990). The location of this borehole is shown in Figure 5.1. The essential data from the borehole are shown in Figure 5.3.

5.3.2 Finite Element Model

Along the cross-section AB shown in Figure 5.1, the behavior of a soil column at the location of borehole BH 88-13 in response to horizontal ground motion would be one dimensional, i.e., little vertical displacement

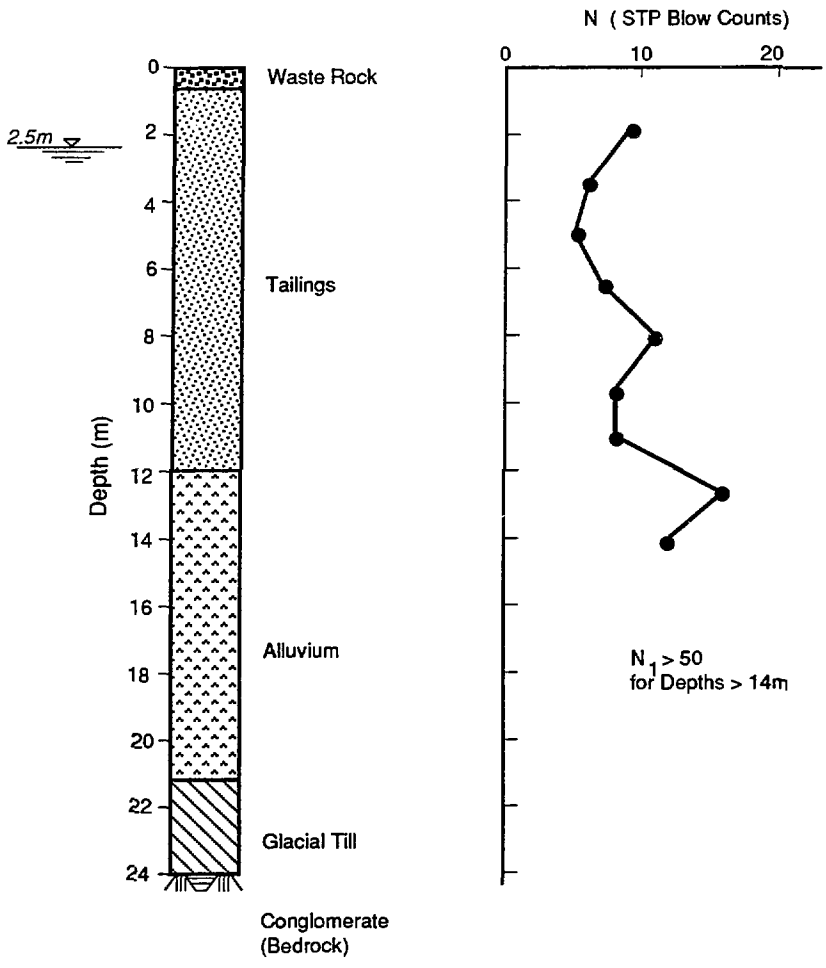

Source: Golder Associates (1990)

Fig. 5.3

Atomic Energy Control Board
Liquefaction of Uranium Tailings
Borehole BH-13 - Lithologic Profile and SPT Test Results

P9296.00Es

is expected due to horizontal motion at the base. For this reason, and also to facilitate better comparison with the borehole data, the one dimensional finite element model shown in Figure 5.4 was used for the total stress analysis.

The model consists of 18 elements and 38 nodes. Vertical displacements are fixed along the sides of the column. Horizontal and vertical displacements are fixed at the base. The base is assumed to be rigid, which is consistent with the presence of bedrock at approximately 24 m. depth in borehole BH 88-13. Two soil types are present in the model: overburden and tailings. The small thickness of glacial till lying above bedrock in BH 88-13 is ignored. Basal till was not observed in any of the other boreholes at the Main Dam and is therefore assumed to be discontinuous (Golder Associates, 1990, p. 20). Material properties for the tailings and overburden are given in Table 5.1. The column was analyzed using the computer program NTSAP described in Section 4.1.

TABLE 5.1

TOTAL STRESS ANALYSIS - MATERIAL PROPERTIES

Property	Tailings	Overburden
ρ (kg/m^3)	1440	2010
n	0.50	0.25
e	1.00	0.33
ρ_{sat} (kg/m^3)	1440	2010
ρ_{dry} (kg/m^3)	940	1770
K_0	0.50	0.50
D_r (%)	40	75
K_2	40	61
ξ	0.30	0.30
ν	0.33	0.33

It should be noted that all of the above properties are estimates based on comparisons with similar materials for which the parameters have been measured. Wide dispersion in the values of these parameters is possible.

5.3.3 Computation of Static Stresses and Initial Moduli

In order to compute the ratio $(\tau/\sigma'_v)_e$ and to compute the initial (small strain) shear modulus G_0 required for NTSAP, the static state of stress must be known. Given the dry and saturated densities shown in Table 5.1 and the soil profile shown in Figure 5.3, the vertical effective stress at a depth z is given by

$$\sigma'_v(z) = \sum_i \rho_i g h_i - p(z) \qquad z = \sum_i h_i$$

where ρ_i is the dry or saturated density (as appropriate) of the soil in a soil column of thickness h_i, g is the

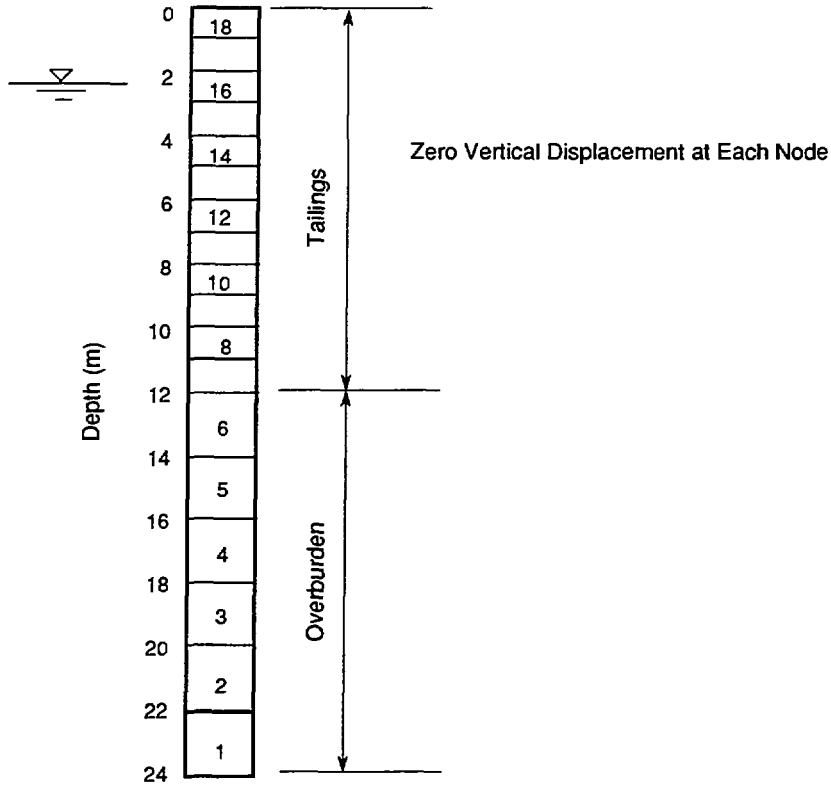

Fig. 5.4

Atomic Energy Control Board
Liquefaction of Uranium Tailings
Finite Element Model - Total Stress Analysis

P929800ES

TABLE 5.2

TOTAL STRESS ANALYSIS - STATIC STRESSES IN SOIL COLUMN

Element	h	σ_v	h_w	p	σ'_v	σ'_m	G_0
18	0.5	4.6	0.0	0.0	4.6	3.1	15.59
17	1.5	13.8	0.0	0.0	13.8	9.2	26.86
16	2.5	23.0	0.0	0.0	23.0	15.4	34.76
15	3.5	37.2	1.0	9.8	27.4	18.3	37.89
14	4.5	51.3	2.0	19.6	31.7	21.2	40.78
13	5.5	65.5	3.0	29.4	36.1	24.1	43.48
12	6.5	79.6	4.0	39.2	40.4	27.0	46.02
11	7.5	93.8	5.0	49.0	44.8	29.9	48.43
10	8.5	107.9	6.0	58.8	49.1	32.8	50.73
9	9.5	122.1	7.0	68.6	53.5	35.7	52.92
8	10.5	136.2	8.0	78.4	57.8	38.6	55.03
7	11.5	150.4	9.0	88.2	62.2	41.5	57.06
6	13.0	177.1	10.5	102.9	74.2	49.5	95.03
5	15.0	216.4	12.5	122.5	93.9	62.6	106.90
4	17.0	255.7	14.5	142.1	113.6	75.7	117.50
3	19.0	295.0	16.5	161.7	133.3	88.9	127.40
2	21.0	334.3	18.5	181.3	153.0	102.0	136.40
1	23.0	373.6	20.5	200.9	172.7	115.1	144.90

All stresses are in kPa. G_0 is in MPa.

acceleration due to gravity, and $p(z)$ is the pore pressure at depth z.† The results of these computations at the centroids of the elements in the finite element model shown in Figure 5.4 are given in Table 5.2.

The mean effective stress is given by

$$\sigma'_m = \frac{\sigma'_v + \sigma'_h + \sigma'_h}{3} = \frac{(1+2K_0)}{3}\sigma'_v$$

where $\sigma'_h = K_0\sigma'_v$, where σ'_h and σ'_v are the horizontal and vertical effective stresses, respectively. K_0 is assumed to be 0.5 in both the tailings and overburden. The results of these computations at the centroids of the elements in the finite element model shown in Figure 5.4 are given in Table 5.2.

The mean effective stress is used to compute the initial (small strain) shear modulus according to the equation

$$G_0 = 22K_2P_a\left(\frac{\sigma'_m}{P_a}\right)^{1/2} \qquad P_a = 101.3 \text{ kPa}$$

where K_2 is a coefficient which depends on the relative density, D_r, of the soil and P_a is the atmospheric pressure. Seed and Idriss (1970) discuss the above equation and provide curves relating K_2 to D_r. The assumed values of D_r and the resulting values of K_2 for both the tailings and the overburden are given in Table 5.1. The computed values of G_0 for each element are given in Table 5.2.

† Estimation of the static stresses in this manner is only possible in a region of zero horizontal flow. Within the dam, for example, seepage forces also contribute to the pore pressure.

5.3.4 Factor of Safety Against Liquefaction

Three iterations were required before the maximum change in modulus in any element was less than 10%. The resulting average shear stresses in each element are given in Table 5.3a. The computation of the induced shear stress ratio $(\tau_{av}/\sigma'_v)_e$ is also given in Table 5.3a.

The original blow count data from the standard penetration tests in borehole BH 88-13 were used to obtain the ratio $(\tau_{av}/\sigma'_v)_s$. If an original datum is denoted N, the standardized blow count N_1 is given by

$$N_1 = C_N N$$

where $C_N = (1/\sigma'_v)^{1/2}$, if σ'_v is in tons/ft^2. The tailings in BH 88-13 can be classified as clean sands since the silt content is less than 10%. Thus no corrections were applied to N_1 to account for the presence of silt. The resulting values of N_1 are shown in Table 5.3b. Values of $(\tau_{av}/\sigma'_v)_s$ were obtained from the curve for M6.0 shown in Figure 1.2. Values of $(\tau_{av}/\sigma'_v)_e$ at the depths of the standard penetration tests were linearly interpolated from the values given in Table 5.3a. The factor of safety against liquefaction could then be computed as shown in Table 5.3b.

The computed factors of safety indicate that for the assumed ground motion and material properties, liquefaction of the tailings would occur to a depth of approximately 11 m. Liquefaction of the overburden below 12.5 m. is not indicated by these results.

The induced shear stress ratio at a depth h can also be computed using Equation 1.6

$$\tau_{av} = 0.65\gamma h a_{max} r_d.$$

The value of a_{max} for the time history shown in Figure 5.2b is 0.15g. Assuming that the tailings in the soil column in Figure 5.3 are saturated at all depths, values of τ_{av} can be computed at three depths shown in Table 5.3b. The results of these calculations are shown below:

$$\begin{array}{llll} h = 3.35 \text{ m} & r_d = 0.98 & \tau_{av} = 4.53 \text{ kPa} & (\tau_{av}/\sigma'_v)_e = 0.17 \\ h = 4.88 \text{ m} & r_d = 0.97 & \tau_{av} = 6.53 \text{ kPa} & (\tau_{av}/\sigma'_v)_e = 0.20 \\ h = 6.40 \text{ m} & r_d = 0.95 & \tau_{av} = 8.39 \text{ kPa} & (\tau_{av}/\sigma'_v)_e = 0.21 \end{array}$$

The values of r_d are taken from Figure 1.1 and the values of σ'_v are taken from Table 5.3b. The above induced shear stress ratios are similar to those shown in Table 5.3b and also indicate liquefaction of the tailings at these depths.

Using the computer program SHAKE, Conlin (1980) analyzed several tailings profiles in the Elliot Lake area and concluded that liquefaction was unlikely in the profiles analyzed. One reason for this conclusion is the assumption of a lower peak ground acceleration, 0.08g versus 0.15g in the present case. Matyas *et al* (1984) assumed the lower peak ground acceleration and used the simplified method for obtaining the induced shear stress ratio and found that liquefaction was likely in localized zones of Elliot Lake tailings. This opposing conclusion may be due to the very soft tailings (SPT blowcounts, N, of 2-3 per foot) present in the boreholes used. It may also be due to the conservative nature of the calculation of induced shear by the simplified method compared with the more rigorous calculation of induced shear using SHAKE.

TABLE 5.3

TOTAL STRESS ANALYSIS

(a) CALCULATION OF INDUCED SHEAR STRESS RATIO

Element	τ_{av}	σ'_v	$(\tau_{av}/\sigma'_v)_e$
18	0.40	4.6	0.09
17	5.21	13.8	0.38
16	6.41	23.0	0.28
15	6.97	27.4	0.25
14	7.03	31.7	0.22
13	7.65	36.1	0.21
12	8.64	40.4	0.21
11	9.77	44.8	0.22
10	9.72	49.1	0.20
9	8.97	53.5	0.17
8	9.18	57.8	0.16
7	9.79	62.2	0.16
6	11.38	74.2	0.15
5	13.48	93.9	0.14
4	13.46	113.6	0.12
3	14.92	133.3	0.11
2	17.75	153.0	0.12
1	19.92	172.7	0.12

All stresses are in kPa.

(b) FACTOR OF SAFETY AGAINST LIQUEFACTION

Depth	σ'_v	N_1	$(\tau_{av}/\sigma'_v)_s$	$(\tau_{av}/\sigma'_v)_e$	FOS
1.83	16.9	14	0.20	0.35	0.57
3.35	26.7	11	0.16	0.25	0.64
4.88	33.4	9	0.13	0.22	0.59
6.40	40.0	11	0.16	0.21	0.76
7.93	46.6	15	0.21	0.21	1.00
9.45	53.3	10	0.14	0.17	0.82
10.98	59.9	10	0.14	0.16	0.88
12.50	69.3	19	0.27	0.16	1.69
14.00	84.1	13	0.18	0.15	1.20
15.55	99.3	94	> 1	0.13	$>> 1$

σ'_v is in kPa.

It is difficult to reconcile these two conclusions since all the data are not available. Also, comparison of the present study with those mentionned above is not be appropriate since the field data are not from the same tailings ponds.

5.4 Effective Stress Analysis

In effective stress analysis, the induced pore pressures are used to determine the onset of liquefacton. If the induced pressures exceed some component of effective stress, then liquefaction can be assumed to have occurred. An effective stress analysis of the tailings at the full pond elevation for the new Main Dam is described below.

5.4.1 Finite Element Model

The two-dimensional finite element model shcwn in Figure 5.5 was used for effective stress analysis using the program NESAP described in Section 4.2. The model is a cross-section along the line AB in Figure 5.1 and includes overburden (12 m. thick), the old Main Dam and tailings to a thickness of 20 m. which corresponds to the maximum pond elevation of the new Main Dam. The model is composed of 127 elements and 148 nodes. Displacements at the 11 nodes along the base are fixed. Displacements at all other nodes are free, resulting in a system of differential equations of order 548.

The accelerogram shown in Figure 5.2 was used as a forcing function. Since it is due to a M6.0 earthquake, the equivalent number of uniform amplitude shear strain cycles is 5 (Seed *et al*, 1976). Pore pressures in the columns labelled C1 and C2 in Figure 5.5 were computed and compared with the initial vertical effective stresses, σ'_v. If the induced pore pressures exceed σ'_v, liquefaction is assumed to have occurred.

5.4.2 Selection of Material Properties

For each material in the finite element model, the following parameters are required:

$$\lambda, G, \rho, n, k, M, K_d.$$

It is assumed that the fluid density $\rho_f = 1000$ kg/m^3 and that $\alpha = 1$.

The bulk densities of the overburden and tailings are assumed to be the same as the densities used in the total stress analysis. The bulk density of the waste rock in the old Main Dam is assumed to be the same as that of the overburden. Values of n, the effective porosity, were assumed for each material. Golder Associates (1990) performed field permeability measurements in overburden and tailings. The permeability of the waste rock was assumed to be the same as that of the tailings. Thus

Material	ρ (kg/m^3)	n	k (m/sec)
Overburden	2010	0.25	10^{-6}
Waste rock	2010	0.25	10^{-5}
Tailings	1440	0.50	10^{-5}

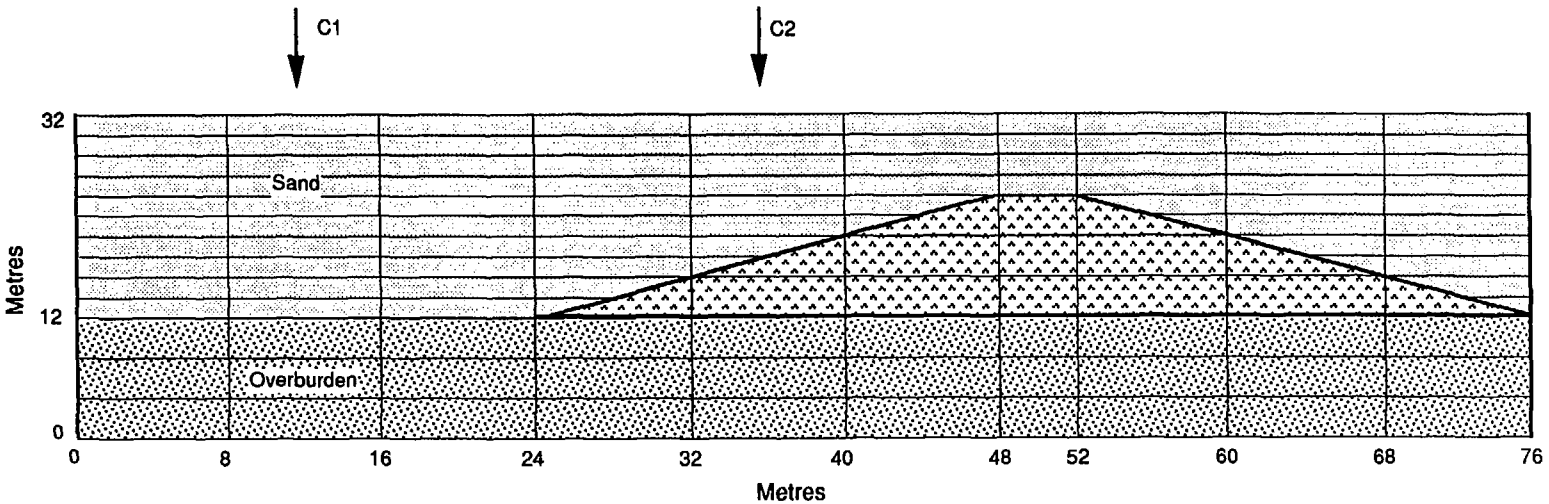

Fig. 5.5

Atomic Energy Control Board
Liquefaction of Uranium Tailings
Finite Element Model - Effective Stress Analysis

ACRES

P9296.00ES

It remains to determine values of the Lamé constants λ and G and the bulk moduli M and K_d. This can be done using the results of seismic refraction surveys done along lines perpendicular to the line AB in Figure 5.1 (Golder Associates, 1990). Line 1 passes through the location of borehole BH 88-13 and Line 2 is along the axis of the old Main Dam.

The P waves produced in the seismic survey are assumed to propagate in saturated porous medium at the velocity V_c given by

$$V_c = \sqrt{\frac{\lambda + 2G + \alpha^2 M}{\rho}} \tag{5.1}$$

Given a measured value of V_c from the refraction survey and a value for ρ, the quantity $\lambda + 2G + \alpha^2 M$ can be computed for the soil type. A further assumption is required to obtain values of $\lambda + 2G$ and M. If the waves propagate such that there is no fluid movement ($w = 0$) then, according to Biot (1962), the following must hold

$$\frac{\alpha M}{\lambda + 2G + \alpha^2 M} = \frac{\rho_f}{\rho}. \tag{5.2}$$

Whether the assumption $w = 0$ is true in practice is debatable; significant relative motion of the pore fluid may not occur due to the short duration impulsive nature of the seismic blast, i.e., the medium moves as a whole.

Equations 5.1 and 5.2 can be used to compute $\lambda + 2G$ and M, given values for all other quantities. To obtain values of λ and G, a value of Poisson's ratio, ν, must be assumed. The quantity $\lambda + 2G$ can then be written as

$$\lambda + 2G = \frac{2G(1-\nu)}{1-2\nu}$$

from which G and then λ may be computed. The value $\nu = 0.3$ was assumed for each material.

Along Line 1, the lowest computed P wave velocity in the overburden was 457 m/sec. Along Line 2, the 'overburden' P wave velocity is actually that of the waste rock in the old Main Dam. At the mid-point of Line 2 its value is 1357 m/sec. Based on the results of the final iteration of the total stress analysis, the shear modulus of the tailings is assumed to be half that of the overburden. Using the appropriate values for ρ and the assumed value of ν, this gives

Material	λ (MPa)	G (MPa)	M (MPa)
Overburden	89.96	59.97	209.9
Waste rock	793.5	528.8	1851.0
Tailings	44.98	29.99	105.0

The values of λ, G and M computed above are for small shear strains, approximately 10^{-4}%, typical of seismic surveys. The total stress analysis described previously and analyses of the response of Santa Felicia dam in California (Abdel-Ghaffar and Scott, 1979) suggest that shear strains on the order of 10^{-2}% are generated in soils during an earthquake. Thus, according to the hyperbolic model, the actual moduli should be less than those computed above. From Table 2.1, the value of G/G_0 for sand at a shear strain of 10^{-2}%

TABLE 5.4

EFFECTIVE STRESS ANALYSIS - MATERIAL PROPERTIES

Material	λ	G	ρ	n	k	M	K_d
Overburden	59.01	39.34	2010	0.25	10^{-6}	137.7	85.24
Waste rock	520.5	346.9	2010	0.25	10^{-5}	1214.0	751.8
Tailings	29.51	19.67	1440	0.50	10^{-5}	68.85	42.62

All moduli are in MPa, all densities are in kg/m^3 and permeabilities are in m/sec.

The damping ratio $\xi = 6\%$.

The constants used in the empirical volumetric strain equation 3.7 were

$$C_1 = 0.80 \quad C_2 = 0.79 \quad C_3 = 0.45 \quad C_4 = 0.73.$$

is 0.656. This reduction applies to values of λ, G and M computed above. Also, from Table 2.1, at this strain level the damping ratio is approximately 6%.

The drained bulk modulus for each material is given by $K_d = \lambda + \frac{2}{3}G$. The material properties for the effective stress analysis are given in Table 5.4.

5.4.3 Induced Pore Pressures in Tailings

Figure 5.6 shows the initial effective vertical stresses in the tailings of columns C1 and C2 shown in Figure 5.5. These stresses were computed using the effective unit weight per meter $9.8(1.44 - 1.0) = 4.31$ kPa/m. The induced pore pressures computed using NESAP are also shown. From this it may be seen that liquefaction is likely only at depths less than 3 m. The induced pore pressures in Column C2 exhibit some irregularities near the boundary between the tailings and waste rock of the old Main Dam. This is likely due to the irregular shape of elements near the boundary.

These results are somewhat sensitive to the assumed material properties, particularly the drained bulk modulus, K_d. A thorough sensitivity study was not done. It should also be noted that NESAP does not have an energy transmitting boundary so that reflections from the model boundaries are present in the response. The effect of these reflections on pore pressure response is not known.

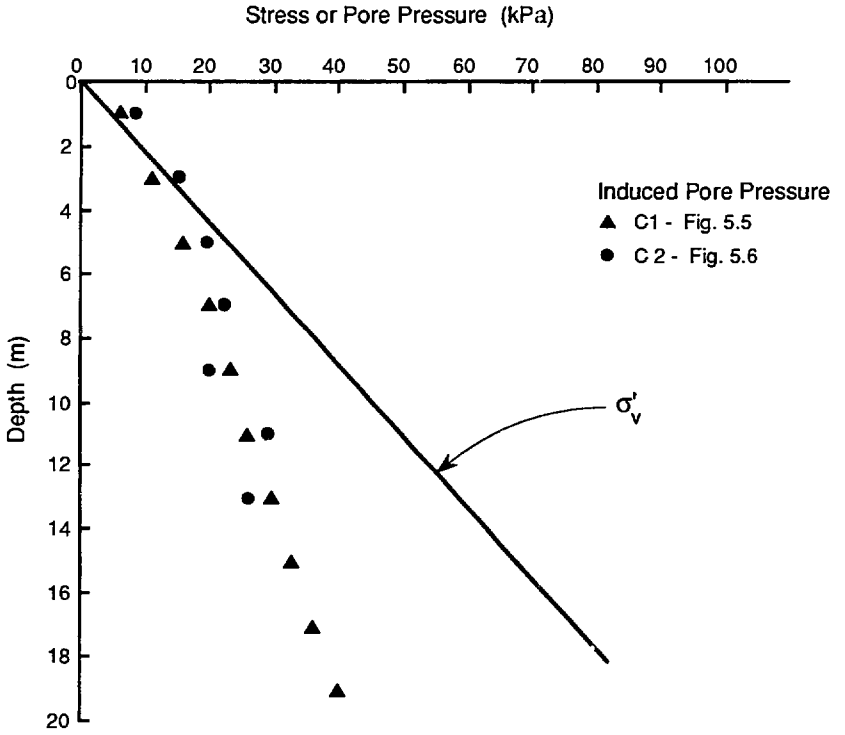

Fig. 5.6

Atomic Energy Control Board
Liquefaction of Uranium Tailings
Induced Pore Pressures in Tailings

ACRES

6.0 CONCLUSIONS AND RECOMMENDATIONS

6.1 Conclusions

Liquefaction analysis of a soil deposit or structure can be done using total stress or effective stress analysis methods. Procedures and computer programs for total stress analysis using the equivalent linear algorithm are well developed and have been used extensively in the past 20 years. Examples include the programs SHAKE and QUAD-4. Non-linear total stress programs are less common.

Practical effective stress analysis programs are still under development. Some uncoupled effective stress schemes for one-dimensional models are available. These models use total stress analysis to compute shear stress time histories which are then used as the forcing function for a pore pressure generation algorithm to compute induced pore pressures. To date, such uncoupled schemes have not been applied in two dimensions.

Practical methods for performing coupled effective stress analysis in two or three dimensions are not available. Considerable research is being done in the development and calibration of such programs, particularly TARA-3 at the University of British Columbia.

It was decided to develop a coupled, two dimensional, effective stress analysis scheme capable of modeling the dynamic behavior of a porous elastic medium. Pore pressure increase during earthquake ground motion is due to both the coupling between the soil skeleton and pore water as well as volume decrease due to shear motion. Of these two mechanisms, the latter is more significant. Volume decrease is an inherently non-linear phenomenon. However, under certain assumptions, the pore pressure increase due to volume decrease can be linearized and computed within a linear analysis. Both mechanisms are included in a computer program called NESAP.

Given NESAP, it was a relatively simple matter to modify it to produce an equivalent linear total stress analysis program. The result was a computer program called NTSAP. It is believed that both these programs constitute a significant contribution to the state of practice.

Both NTSAP and NESAP were appled to the analysis of the liquefaction susceptibility of tailings deposited in the tailings disposal area of the Quirke Uranium Mine near Elliot Lake, Ontario. The assumed ground motion in both analyses was the accelerogram recorded during the 1988 M6.0 Saguenay, Quebec earthquake. The total stress analysis was done on a one-dimensional column model of the tailings as of 1988. The total height of tailings was 12 metres. Borehole standard penetration tests were used to obtain values of resistance to liquefaction. The total stress analysis gave values of induced shear stress. Factors of safety against liquefaction could then be computed. These revealed that liquefaction was possible in the upper 11 metres of tailings. The results agreed with a simplified analysis used to compute induced shear.

An effective stress analysis was done on a two-dimensional model of the tailings at the maximum pond elevation corresponding to the new Main Dam. The total height of tailings at the central portion of the pond was 20 metres. The results of this analysis did not indicate extensive liquefaction of the tailings. Only the upper 3 metres of tailings would be susceptible to liquefaction.

These conclusions regarding the liquefaction susceptibility of the tailings must be qualified as follows.

1) The assumed accelerogram is likely conservative for the region. In time history analyses such as described herein, the peak acceleration does not mean much in terms of response. However, the duration of strong ground is significant to the computed response. Duration tends to increase with earthquake magnitude. The question is, therefore, whether the magnitude of the earthquake, M6.0, which caused the accelerogram is appropriate.

2) The results are sensitive to the selected material properties. This is particularly true of the effective stress analysis where there is considerable uncertainty in the assumed material properties.

3) The results apply only to a small part of the tailings disposal area. The behavior of tailings in other areas would likely be different, particularly areas with significant quantities of silty tailings which exhibit cohesion and may therefore be more resistant to liquefaction.

6.2 Recommendations

The following recommendations for future work can be made.

1) More thorough liquefaction analyses of the tailings should be done in other parts of the disposal area. These analyses could take advantage of more recent borehole and laboratory data and would help address the uncertainty due to tailings composition.

2) A suite of time histories due to different magnitude earthquakes should be used in any future time history analysis in order to obtain a range of expected response.

3) Neither of the newly developed codes NTSAP and NESAP is in production form. Relatively little effort would be required to make the codes more usable and to produce user's manuals.

4) The effect of pore pressure increase due to densification is included in NESAP in a rather ad hoc fashion. A more rigorous approach could be developed in which the pore pressure increases due to densification are computed during the solution process. This would circumvent establishing equivalent numbers of cycles and amplitudes due to a given earthquake magnitude. Alternatively, a non-linear model which includes pore pressure increase due to densification could be implemented in NESAP.

5) An energy transmitting boundary should be implemented in both NTSAP and NESAP.

6) Although containment structures such as the new Main Dam are well engineered, their stability in the event of liquefied tailings should be checked.

REFERENCES

Abdel-Ghaffar, A. M. and Scott, R. F., 1979. Shear moduli and damping factors of earth dam, *Journal of Geotechnical Engineering, ASCE*, **105(GT12)**, 1405-1426.

Ballard, R. F. and McLean, F. G., 1975. *Seismic Field Methods for In Situ Moduli*, Misc. Paper S-75-10, U. S. Army Engineer Waterways Experiment Station, Vicksburg, Miss.

Bathe, K. J., 1982. *Finite Element Procedures in Engineering Analysis*, Prentice-Hall.

Bazant, Z. P. and Krizek, R. J., 1975. Saturated sand as an inelastic two-phase medium, *Journal of Engineering Mechanics, ASCE*, **101(EM4)**, 317-332.

Biot, M. A., 1962. Generalized theory of acoustic propagation in porous dissipative media, *Journal of the Acoustical Society of America*, **34**, 1254-1264.

Booker, J. R., Rahman, M. S. and Seed, H. B., 1976. *GADFLEA: A Computer Program for the Analysis of Pore Pressure Generation and Dissipation During Cyclic or Earthquake Loading*, Report EERC 76-24, Earthquake Engineering Research Center, Berkeley, Ca.

Chugh, A. K. and Von Thun, J. L., 1985. Pore pressure response analysis for earthquakes, *Canadian Geotechnical Journal*, **22**, 466-476.

Conlin, B., 1980. *Design Considerations for Earthquake-Resistant Mine Tailings Impoundment Structures in Northern Ontario*, M.A.Sc. thesis, Department of Civil Engineering, University of Toronto.

Dikmen, S. U. and Ghaboussi, J., 1984. Effective stress analysis of seismic response and liquefaction: theory, *Journal of Geotechnical Engineering, ASCE*, **110(GT5)**, 628-644.

Duncan, J. M. and Chang, C. Y., 1970. Nonlinear analysis of stress and strain in soils, *Journal of the Soil Mechanics and Foundations Division, ASCE*, **96(SM5)**, 1629-1653.

Ferrito, J. M. and Nakamoto, R. T., 1984. *A Summary of the Prevost Effective Stress Soil Model*, Technical Report R-913, Naval Civil Engineering Laboratory, Port Hueneme, Ca.

Finn, W. D. L., 1985. Dynamic effective stress response of soil structures: theory and centrifugal model studies. In Proceedings 5th International Conference on Numerical Methods in Geomechanics, Nagoya, Japan. Vol. 1, pp. 35-46.

Finn, W. D. L., 1987. Estimating liquefaction potential by analysis. In Proceedings 2nd International Conference on Constitutive Laws for Engineering Materials, University of Arizona, Tucson, Az.

Finn, W. D. L., Lee, K. W. and Martin, G. R., 1977. An effective stress model for liquefaction, *Journal of Geotechnical Engineering, ASCE*, **103(GT6)**, 517-533.

Finn, W. D. L., Siddharthan, R., Lee, F., and Schofield, A. N., 1984. Seismic response of offshore drilling islands in a centrifuge including soil-structure interaction. In Proceedings 16th Annual Offshore Technology Conference, Houston, Texas.

Finn, W. D. L., Yogendrakumar, M., Yoshida, N. and Yoshida, H., 1986. *TARA-3: A Program for Non-linear Static and Dynamic Effective Stress Analysis*, Soil Mechanics Group, University of British Columbia, Vancouver, B. C.

Ghaboussi, J. and Dikmen, S. U., 1978. Liquefaction analysis of horizontally layered sands, *Journal of Geotechnical Engineering, ASCE*, **104(GT3)**, 341-356.

Ghaboussi, J. and Dikmen, S. U., 1984. Effective stress analysis of seismic response and liquefaction: case studies, *Journal of Geotechnical Engineering, ASCE*, **110(GT5)**, 645-658.

Ghaboussi, L. and Wilson, E. L., 1972. Variational formulation of dynamics of fluid-saturated porous elastic solids, *Journal of Engineering Mechanics, ASCE*, **98(EM4)**, 947-963.

Ghaboussi, J. and Wilson, E. L., 1973. Seismic analysis of earth dam-reservoir systems, *Journal of the Soil Mechanics and Foundations Division, ASCE*, **99(SM10)**, 849-862.

Golder Associates, 1990. *Geotechnical Investigations and Design Recommendations, Main Dam Remediation, Quirke Mine Tailings Impoundment*, Report to Rio Algom Ltd., Golder Associates, Mississauga, Ont.

Griffiths, D. V. and Prevost, J. H., 1988. Two and Three-dimensional dynamic finite element analyses of the Long valley dam, *Geotechnique*, **38**, 367-388.

Hardin, B. O. and Drnevich, V. P., 1972. Shear modulus and damping in soils: measurement and parameter effects, *Journal of the Soil Mechanics and Foundations Division, ASCE*, **98(SM6)**, 603-624.

Hughes, T. J. R., 1987. *The Finite Element Method*, Prentice-Hall.

Idriss, I. M., Lysmer, J., Hwang, R. and Seed, H. B., 1973. *QUAD-4: A Computer Program for Evaluating the Seismic Response of Soil Structures by Variable Damping Finite Element Procedures*, Report EERC 73-16, Earthquake Engineering Research Center, Berkeley, Ca.

Ishihara, K., 1986. Evaluation of soil properties for use in earthquake response analysis. In *Numerical Models in Engineering Practice*, Chapter 10 (R. Dungar and J. A. Stuger, eds.), A. A. Balkema.

Ishihara, K. and Towhata, I., 1980. One-dimensional soil response analysis during earthquakes based on effective stress method. Journal of the Faculty of Engineering, University of Tokyo, **35(4)**.

Ishihara, K., Tatsuoka, F., and Yasuda, S., 1975. Undrained deformation and liquefaction of sand under cyclic stresses, *Soils and Foundations*, **15**, 29-44.

Kishida, H., 1966. Damage to reinforced concrete buildings in Niigata city with special reference to foundation engineering, *Soils and Foundations*, **7**, 71-88.

Koizumi, Y., 1966. Changes in density of sand subsoil caused by the Niigata earthquake, *Soils and Foundations*, **6**, 38-44.

Kondner, R. L. and Zelasko, J. S., 1963. A hyperbolic stress-strain formulation of sands. In Proceedings of 2nd Pan American Conference on Soil Mechanics and Foundation Engineering (Brazil), pp. 289-324.

Kovacs, W. D., Salamone, L. A. and Yokel, F. Y., 1983. *Comparison of Energy Measurements in teh Standard Penetration Test using the Cathead and Rope Method*, Report to US Nuclear Regulatory Commission, National Bureau of Standards.

Lee, K. L. and Chan, K., 1972. Number pf equivalent significant cycles in strong motion earthquakes. In Proceedings International Conference on Microzonation, Seattle, Wash., v. 11, pp. 609-627.

Lee, M. K. W. and Finn, W. D. L., 1975. *DESRA-1: Program for the Dynamic Effective Stress Response Analysis of Soil Deposits Including Liquefaction Evaluation*, Report No. 36, Soil Mechanics Series, Department of Civil Engineering, University of British Columbia, Vancouver, B. C.

Lee, M. K. W. and Finn, W. D. L., 1978. *DESRA-2: Dynamic Effective Stress Response Analysis of Soil Deposits with Energy Transmitting Boundary Including Assessment of Liquefaction Potential*, Report No. 38, Soil Mechanics Series, Department of Civil Engineering, University of British Columbia, Vancouver, B. C.

Liao, S. and Whitman, R. V., 1986. Overburden correction factors for SPT in sand, *Journal of Geotechnical Engineering, ASCE*, **112(GT3)**, 373-377.

Liou, C. P., Streeter, V. L. and Richart, F. E., 1977. A numerical model for liquefaction, *Journal of Geotechnical Engineering, ASCE*, **103(GT6)**, 589-606.

Lysmer, J., Udaka, T., Seed, H. B. and Hwang, R., 1974. *LUSH: A Computer Program for Complex Response Analysis of Soil-Structure Systems*, Report EERC 74-4, Earthquake Engineering Research Center, Berkeley, Ca.

Lysmer, J., Udaka, T., Tsai, C. F. and Seed H. B., 1975. *FLUSH: A Computer Program for Approximate 3-D Analysis of Soil-Structure Interaction Problems*, Report EERC 75-30, Earthquake Engineering Research Center, Berkeley, Ca.

Mansouri, T. A., 1980. *Dynamic Response and Liquefaction of Earth Structures*, Ph.D. Dissertation, Department of Civil Engineering, Colorado State University, Fort Collins, Colo.

Mansouri, T. A., Nelson, J. D. and Thompson, E. G., 1983. Dynamic response and liquefaction of earth dams, *Journal of Geotechnical Engineering, ASCE*, **109(GT1)**, 89-100.

Martin, P. P., 1978. *A Computer Program for the Non-linear Analysis of Vertically Propagating Shear Waves in Horizontally Layered Deposits*, Report EERC 78-23, Earthquake Engineering Research Center, Berkeley, Ca.

Martin, P. P. and Seed, H. B., 1978. *APOLLO: A Computer Program for the Analysis of Pore Pressure Generation and Dissipation in Horizontal Sand Layers During Cyclic or Earthquake Loading*, Report EERC 78-21, Earthquake Engineering Research Center, Berkeley, Ca.

Martin, P. P. and Seed, H. B., 1979. Simplified procedure for effective stress analysis of ground response, *Journal of Geotechnical Engineering, ASCE*, **105(GT6)**, 739-758.

Martin, G. R., Finn, W. D. L. and Seed, H. B., 1975. Fundamentals of liquefaction under cyclic loading, *Journal of Geotechnical Engineering, ASCE*, **101(GT5)**, 423-438.

Matyas, E. L., Welch, D. E. and Reades, D. W., 1984. Geotechnical parameters and behavior of uranium tailings, *Canadian Geotechnical Journal*, **21**, 489-504.

Ohsaki, Y., 1966. Niigata earthquakes, 1964 building damage and conditions, *Soils and Foundations*, 6, 14-37.

Prevost, J. H., 1978. Plasticity theory for soil stress-strain behavior, *Journal of Engineering Mechanics, ASCE*, **104(EM5)**, 1177-1194.

Prevost, J. H., 1982. Non-linear transient phenomena in saturated porous media, *Computer Methods in Applied Mechanics and Engineering*, **30**, 3-18.

Prevost, J. H., 1983. *DYNAFLOW - User's Manual*, Department of Civil Engineering, Princeton University.

Pyke, R. M., 1979. Nonlinear soil model for irregular cyclic loadings, *Journal of Geotechnical Engineering, ASCE*, **105(GT5)**, 715-726.

Schnabel, P. B., Lysmer, J. and Seed, H. B., 1972. *SHAKE: A Computer Program for Earthquake Response Analysis of Horizontally Layered Sites*, Report EERC 72-12, Earthquake Engineering Research Center, Berkeley, Ca.

Seed, H. B. and Idriss, I. M., 1969. Influence of soil conditions on ground motions during earthquakes, *Journal of the Soil Mechanics and Foundations Division, ASCE*, **95(SM1)**, 99-137.

Seed, H. B. and Idriss, I. M., 1970. *Soil Moduli and Damping Factors for Dynamic Response Analysis*, Report EERC 70-10, Earthquake Engineering Research Center, Berkeley, Ca.

Seed, H. B. and Idriss, I. M., 1971. Simplified procedure for evaluating soil liquefaction potential, *Journal of the Soil Mechanics and Foundations Division, ASCE*, **97(SM9)**, 1249-1273.

Seed, H. B. and Idriss, I. M., 1982. *Ground Motion and Soil Liquefaction During Earthquakes*, Earthquake Engineering Research Institute, Berkeley, Ca.

Seed, H. B., Idriss, I. M. and Arango, I., 1983. Evaluation of liquefaction potential using field performance data, *Journal of Geotechnical Engineering, ASCE*, **109(GT3)**, 458-482.

Seed, H. B., Idriss, I. M., Makdisi, F. and Banerjee, N., 1975. *Representation of Irregular Stress Time Histories by Equivalent Uniform Stress Series in Liquefaction Analyses*, Report EERC 75-29, Earthquake Engineering Research Center, Berkeley, Ca.

Seed, H. B. and Lee, K. L., 1966. Liquefaction of Saturated Sands During Cyclic Loading, *Journal of the Soil Mechanics and Foundations Division, ASCE*, **92(SM6)**, 105-134.

Seed, H. B., Martin, P. P. and Lysmer, J., 1976. Pore-water pressure changes during soil liquefaction, *Journal of Geotechnical Engineering, ASCE*, **102(GT4)**, 323-346.

Seed, H. B. and Peacock, W. H., 1971. Test Procedures for Measuring Soil Liquefaction Characteristics, *Journal of the Soil Mechanics and Foundations Division, ASCE*, **97(SM8)**, 1099-1119.

Seed, H. B., Tokimatsu, K., Harder, L. F. and Chung, R. M., 1985. Influence of SPT procedures in soil liquefaction, *Journal of Geotechnical Engineering, ASCE*, **111(GT12)**, 1425-1445.

Seed, H. B., Wong, R. T., Idriss, I. M. and Tokimatsu, K., 1986. Moduli and damping factors for dynamic analyses of cohesionless soils, *Journal of Geotechnical Engineering, ASCE*, **112**, 1016-1032.

Silver, M. L., 1980. *Cyclic Strength of Reconstituted Shell Sands and Till Core Materials*, Report to Denison Mines Ltd., M. L. Silver, University of Illinois.

Simon, B. R., Zienkiewicz, O. C. and Paul, D. K., 1984. An analytical solution for the transient response of saturated porous elastic solids, *International Journal for Numerical and Analytical Methods in Geomechanics*, **8**, 381-398.

Wilson, E. L. and Clough, R. W., 1962. Dynamic response by step-by-step matrix analysis. In *Proceedings of Symposium on Use of Computers in Civil Engineering*, Lisbon.

Zienkiewicz, O. C., 1977. *The Finite Element Method*, Third Edition, McGraw-Hill.

APPENDIX I

FINITE ELEMENT MATRICES

Expressions for the element matrices used to construct the global matrices in Equations 1.1 and 3.3 are given below. Plane strain conditions and uniform material properties within an element are assumed. The shape functions are those of a four-noded isoparametric quadrilateral shown in Figure A.1 (Bathe, 1982).

Equation 1.1

Assume the element nodal displacements are arranged in a vector as follows

$$\mathbf{u} = [u_x^1, u_y^1, \ldots, u_x^4, u_y^4]^t$$

where the superscript denotes the node number. The element mass and stiffness matrices of Equation 1.1 are then given by

$$\begin{aligned}\mathbf{m} &= \rho \int_V \mathbf{H}^t\mathbf{H}\, dV \\ &= \rho \int_{-1}^{1}\int_{-1}^{1} \mathbf{H}^t\mathbf{H} J(r,s)\, dr\, ds \\ \mathbf{k} &= \int_V \mathbf{B}^t\mathbf{D}\mathbf{B}\, dV \\ &= \int_{-1}^{1}\int_{-1}^{1} \mathbf{B}^t\mathbf{D}\mathbf{B} J(r,s)\, dr\, ds\end{aligned}$$

The definitions of the terms in these expressions are given below. **H** is a matrix of shape functions

$$\mathbf{H} = \begin{bmatrix} h_1 & 0 & h_2 & 0 & h_3 & 0 & h_4 & 0 \\ 0 & h_1 & 0 & h_2 & 0 & h_3 & 0 & h_4 \end{bmatrix},$$

where

$$\begin{aligned} h_1 &= \frac{1}{4}(1+r)(1+s) \\ h_2 &= \frac{1}{4}(1-r)(1+s) \\ h_3 &= \frac{1}{4}(1-r)(1-s) \\ h_4 &= \frac{1}{4}(1+r)(1-s) \end{aligned}$$

$J(r,s)$ is the Jacobian determinant

$$J(r,s) = \begin{vmatrix} x_{,r} & y_{,r} \\ x_{,s} & y_{,s} \end{vmatrix}$$

where

$$x = \sum_i h_i x^i \qquad y = \sum_i h_i y^i.$$

B is a matrix of shape function derivatives such that $\mathbf{e} = \mathbf{B}\mathbf{u}$ or

$$\mathbf{e} = \begin{bmatrix} \epsilon_{xx} \\ \epsilon_{yy} \\ \epsilon_{xy} \end{bmatrix} = \mathbf{B}\mathbf{u} = \begin{bmatrix} h_{1,x} & 0 & h_{2,x} & 0 & h_{3,x} & 0 & h_{4,x} & 0 \\ 0 & h_{1,y} & 0 & h_{2,y} & 0 & h_{3,y} & 0 & h_{4,y} \\ h_{1,y} & h_{1,x} & h_{2,y} & h_{2,x} & h_{3,y} & h_{3,x} & h_{4,y} & h_{4,x} \end{bmatrix} \begin{bmatrix} u_x^1 \\ u_y^1 \\ \vdots \\ u_x^4 \\ u_y^4 \end{bmatrix}$$

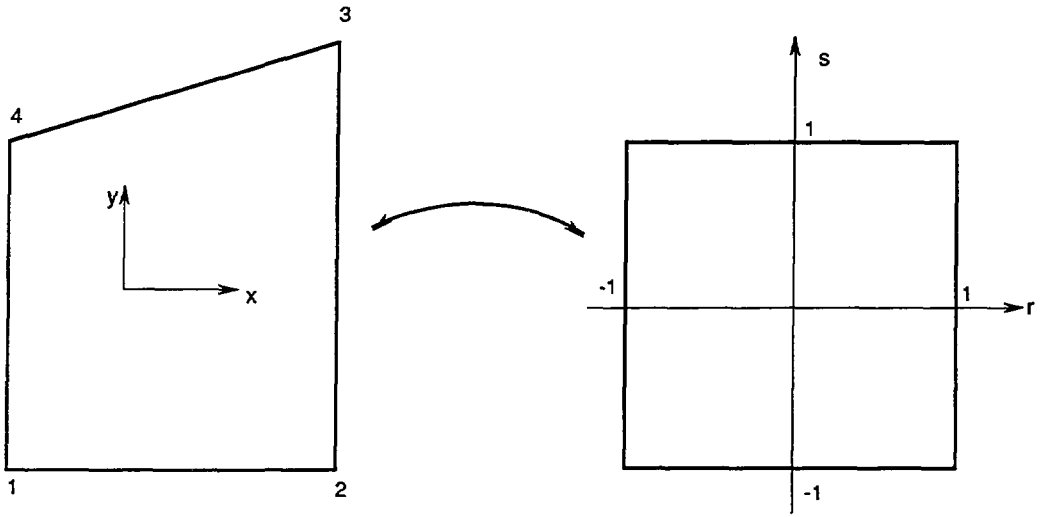

Fig. A.1

Atomic Energy Control Board
Liquefaction of Uranium Tailings
Four Node Isoparametric Quadrilateral

ACRES

P9296.00ES

D is a matrix of elastic constants corresponding to plane strain and such that s = **D**e or

$$\mathrm{s} = \begin{bmatrix} \sigma_{xx} \\ \sigma_{yy} \\ \sigma_{xy} \end{bmatrix} = \mathbf{D}\mathrm{e} = \begin{bmatrix} \lambda + 2G & \lambda & 0 \\ \lambda & \lambda + 2G & 0 \\ 0 & 0 & 2G \end{bmatrix} \begin{bmatrix} \epsilon_{xx} \\ \epsilon_{yy} \\ \epsilon_{xy} \end{bmatrix}$$

Equation 3.3

Assume the element nodal displacements of the solid and liquid phases are arranged in a vector as follows

$$\mathbf{u} = [u_x^1, w_x^1, u_y^1, w_y^1, \ldots, u_x^4, w_x^4, u_y^4, w_y^4]^t$$

where the superscript denotes the node number. The element matrices of Equation 3.3 are then given by

$$\mathbf{m}_s = \rho \int_V \mathbf{H}^t\mathbf{H}\, dV$$

$$\mathbf{m}_f = \frac{\rho_f}{n} \int_V \mathbf{H}^t\mathbf{H}\, dV$$

$$\mathbf{m}_c = \rho_f \int_V \mathbf{H}^t\mathbf{H}\, dV$$

$$\mathbf{c}_f = \frac{1}{k} \int_V \mathbf{H}^t\mathbf{H}\, dV$$

$$\mathbf{k}_s = \int_V (\mathbf{B}^t\mathbf{D}\mathbf{B} + \alpha^2 M \mathbf{A}^t\mathbf{A})\, dV$$

$$\mathbf{k}_f = M \int_V \mathbf{A}^t\mathbf{A}\, dV$$

$$\mathbf{k}_c = \alpha M \int_V \mathbf{A}^t\mathbf{A}\, dV$$

The integration over the quadrilateral follows exactly the same scheme as that for the matrices of Equation 1.1. **A** is a vector of derivatives of shape functions such that $\theta = \mathbf{A}\mathbf{w}$ or

$$\theta = w_{x,x} + w_{y,y} = \mathbf{A}\mathbf{w} = [h_{1,x} \quad h_{1,y} \quad \ldots, \quad h_{4,x} \quad h_{4,y}] \begin{bmatrix} w_x^1 \\ w_y^1 \\ \vdots \\ w_x^4 \\ w_y^4 \end{bmatrix}$$

The matrix **D** of elastic constants is the same as for Equation 1.1 except that the Lamé constants λ and G are for drained conditions.

APPENDIX II

ELASTIC CONSTANTS FOR POROUS SATURATED MEDIUM

Expressions for the elastic constants M and α for a porous medium are derived in Simon *et al* (1984). In three dimensions, let the vector $\mathbf{s} = (\sigma_{xx}, \sigma_{yy}, \sigma_{zz}, \sigma_{xy}, \sigma_{yz}, \sigma_{xz})^t$ and the vector $\mathbf{e} = (\epsilon_{xx}, \epsilon_{yy}, \epsilon_{zz}, \epsilon_{xy}, \epsilon_{yz}, \epsilon_{xz})^t$. The constitutive relationship Equation 3.2a can then be written as

$$\boldsymbol{s} = \mathbf{D}\mathbf{e} + \alpha M p \tag{II.1}$$

where $\mathbf{D}$ is a tensor of drained elastic constants

$$\mathbf{D} = \begin{bmatrix} \lambda+2G & \lambda & \lambda & 0 & 0 & 0 \\ \lambda & \lambda+2G & \lambda & 0 & 0 & 0 \\ \lambda & \lambda & \lambda+2G & 0 & 0 & 0 \\ 0 & 0 & 0 & 2G & 0 & 0 \\ 0 & 0 & 0 & 0 & 2G & 0 \\ 0 & 0 & 0 & 0 & 0 & 2G \end{bmatrix}.$$

From the definition of effective stress

$$\boldsymbol{s}' = \boldsymbol{s} - \mathbf{v}p = \mathbf{D}\boldsymbol{e}' = \mathbf{D}\left(\mathbf{e} - \frac{\mathbf{v}^t\mathbf{e}}{3}\right) \tag{II.2}$$

where $\mathbf{v} = (1,1,1,0,0,0)^t$. Since $\mathbf{v}^t\mathbf{e}/3 = p/3K_s$, where K_s is the bulk modulus for the solid matrix,

$$\boldsymbol{s} = \mathbf{D}\mathbf{e} + \left(\mathbf{v} - \frac{\mathbf{D}\mathbf{v}}{3K_s}\right)p \tag{II.3}$$

Comparison of Equation II.3 with II.1 gives

$$\alpha\mathbf{v} = \mathbf{v} - \frac{\mathbf{D}\mathbf{v}}{3K_s} \tag{II.4}$$

Premultiplying Equation II.4 by $\mathbf{v}^t$ and noting that $\mathbf{v}^t\mathbf{v} = 3$, an expression for α is obtained

$$\alpha = 1 - \frac{\mathbf{v}^t\mathbf{D}\mathbf{v}}{9K_s} = 1 - \frac{K_d}{K_s} \tag{II.5}$$

where K_d is the drained bulk modulus $K_d = \lambda + \frac{2}{3}G$. For most soils, $K_s >> K_d$, i.e., the soil grains are incompressible, and $\alpha = 1$.

Using the time derivative of the constitutive relationship Equation 3.2b, one can obtain an expression for M. The rate of fluid accumulation $\dot{\theta}$ is given by

$$\dot{\theta} = -\alpha\mathbf{v}^t\dot{\mathbf{e}} + \frac{\dot{p}}{M} \tag{II.6}$$

where the dot denotes a time derivative. There are four contributions to $\dot{\theta}$:

1) the rate of change of volumetric strain in the solid

$$-\mathbf{v}^t\dot{\mathbf{e}}$$

2) the rate of change due to compression of the solid by $\dot{p}$

$$\frac{(1-n)\dot{p}}{K_s}$$

3) the rate of change due to compression of the solid by $\mathbf{v}^t\dot{\sigma}'$ which, using Equation II.2, is given by

$$\frac{\mathbf{v}^t\dot{\sigma}'}{3K_s} = \frac{\mathbf{v}^t\mathbf{D}\dot{\mathbf{e}}'}{3K_s} = \frac{\mathbf{v}^t\mathbf{D}\dot{\mathbf{e}}}{3K_s} - \frac{\mathbf{v}^t\mathbf{D}\mathbf{v}}{9K_s^2}\dot{p}$$

4) the rate of change due to compressibility of the pore fluid

$$\frac{n\dot{p}}{K_f}$$

where K_f is the bulk modulus of the pore fluid.

Adding each of these contributions gives

$$\dot{\theta} = -\left(\mathbf{v}^t - \frac{\mathbf{v}^t\mathbf{D}}{3K_s}\right)\dot{\mathbf{e}} + \left(\frac{n}{K_f} + \frac{1-n}{K_s} + \frac{\mathbf{v}^t\mathbf{D}\mathbf{v}}{9K_s^2}\right)\dot{p} \tag{II.7}$$

Comparison of Equation II.7 and II.6 gives

$$\frac{1}{M} = \frac{n}{K_f} + \frac{1-n}{K_s} - \frac{\mathbf{v}^t\mathbf{D}\mathbf{v}}{9K_s^2} \tag{II.8}$$

which, using Equation II.5, can be rewritten as

$$\frac{1}{M} = \frac{n}{K_f} + \frac{\alpha - n}{K_s} \tag{II.9}$$

For incompressible soil, $K_s >> K_f$ and

$$M = \frac{K_f}{n} \tag{II.10}$$

APPENDIX III

PORE PRESSURE INCREASE DUE TO DENSIFICATION

If undrained conditions prevail during an earthquake, no volume chnage occurs and the sum of the elastic and inealstic strain increments is zero, i.e.,

$$\Delta\epsilon + \Delta\epsilon^p = 0. \tag{III.1}$$

The total normal stresses at any point are therefore constant or

$$\sigma_{xx} + \sigma_{yy} + \sigma_{zz} = 0.$$

From Equation 3.2a

$$\sigma_{ij} = (\lambda + \alpha^2 M)\epsilon\delta_{ij} + 2G\epsilon_{ij} + \alpha M\theta\delta_{ij}$$

Assuming $\alpha = 1$ and adding the normal stresses

$$0 = (3\lambda + M)\epsilon + 2G\epsilon + 3M\theta$$

from which

$$M\theta = -\frac{1}{3}[2G + (3\lambda + M)]\epsilon$$

which, using Equation III.1, implies that

$$M\Delta\theta^p = \frac{1}{3}[2G + 3(\lambda + M)]\Delta\epsilon^p \tag{III.2}$$

From Equation 3.2b with $\alpha = 1$

$$p = M(\epsilon + \theta)$$

or

$$\Delta p = -M\Delta\epsilon^p + M\Delta\theta^p$$

Substituting for $M\Delta\theta^p$ from Equation III.2 gives

$$\Delta p = -M\Delta\epsilon^p + \frac{1}{3}[2G + 3(\lambda + M)]\Delta\epsilon^p$$

Since $K_d = \lambda + \frac{2}{3}G$,

$$\begin{aligned}\Delta p &= -M\Delta\epsilon^p + \frac{1}{3}[2G + 3K_d - 2G + 3M]\Delta\epsilon^p \\ &= K_d\Delta\epsilon^p\end{aligned} \tag{III.3}$$

A similar derivation was given by Mansouri (1980). Bazant and Krizek (1975) derived the relationship in a different manner.